

Searching for Radio Transients with Inverted Spectra in Epoch 1 of VLASS and VCSS, and Identification of a Sample of Candidate Relativistic Nuclear Transients

YUYANG CHEN ^{1,2} B. M. GAENSLER ^{2,1,3} TRACY CLARKE ⁴ WENDY PETERS ⁴ EMIL POLISENSKY ⁴ AND KOVI ROSE ^{5,6}

¹*David A. Dunlap Department of Astronomy & Astrophysics, University of Toronto, Toronto, ON M5S 3H4, Canada*

²*Dunlap Institute for Astronomy & Astrophysics, University of Toronto, Toronto, ON M5S 3H4, Canada*

³*Department of Astronomy and Astrophysics, University of California Santa Cruz, Santa Cruz, CA 95064, USA*

⁴*U.S. Naval Research Laboratory, 4555 Overlook Ave. SW, Washington, DC 20375, USA*

⁵*Sydney Institute for Astronomy, School of Physics, University of Sydney, NSW, 2006, Australia*

⁶*CSIRO Space and Astronomy, PO Box 76, Epping, NSW, 1710, Australia*

ABSTRACT

For radio transients, an inverted spectrum (defined as $\alpha > 0$ for a power law spectrum $S_\nu \propto \nu^\alpha$) constrains physical properties, which in principle can be a useful criterion for selecting specific targets of interest in a transient search. To test and develop this concept, we have searched epoch 1 of the Very Large Array Sky Survey (VLASS; 3.0 GHz) and the VLITE Commensal Sky Survey (VCSS; 340 MHz) for radio transients with inverted spectra. We discover a sample of 22 inverted-spectra transient candidates that are not associated with cataloged active galactic nuclei (AGNs). To the best of our knowledge, none of our candidates have transient counterparts at other wavelengths, and only one has previously been reported as a radio transient. We find that our candidates evolve slowly over years and show either highly inverted spectra or peaked spectra over $\sim 1\text{--}3$ GHz. Within our sample, nine candidates are matched to optical centers of galaxies and have estimated radio spectral luminosities of $L_{3.0\text{GHz}} \sim 10^{30} - 10^{33} \text{ erg s}^{-1} \text{ Hz}^{-1}$. Based on the observed properties, we find the most plausible transient classification for our candidates to be relativistic tidal disruption events. However, we are unable to fully rule out variable or transient AGNs with highly inverted spectra. Upon examining physical constraints, we confirm that mainly relativistic transients (on-axis or off-axis) with equipartition energy $E_{\text{eq}} \gtrsim 10^{49} - 10^{53} \text{ erg}$ are expected from searching VLASS and VCSS based on inverted spectra. The obtainable physical constraints, however, can be weak due to degeneracy introduced by viewing angle.

1. INTRODUCTION

Transient phenomena such as supernovae (SNe), tidal disruption events (TDEs), and gamma-ray burst (GRB) afterglows are known to produce slow-evolving radio synchrotron emission from shock-accelerated particles (e.g., Chandra & Frail 2012; Alexander et al. 2020; Bietenholz et al. 2021). These phenomena therefore also manifest as slow¹ transients at radio frequencies. Such radio synchrotron emission contains valuable information regarding the energetics, surrounding environment, and emission size of the transient, offering a unique per-

spective of the physical processes involved (Chevalier 1998; Granot & Sari 2002; Barniol Duran et al. 2013).

In the past, the study of (slow) transients at radio frequencies relied heavily on follow-up observations of events discovered by optical and X-ray telescopes. Now, new generations of wide-field radio sky surveys are enabling systematic discoveries of radio transients. To provide some examples, the Australian SKA Pathfinder (ASKAP; Johnston et al. 2007; Hotan et al. 2021) has been conducting surveys such as the Rapid ASKAP Continuum Survey (RACS; McConnell et al. 2020; Hale et al. 2021; Duchesne et al. 2023a) and the Variable and Slow Transients survey (VAST; Murphy et al. 2013, 2021) over selected frequencies spanning $\nu \simeq 0.7\text{--}1.8$ GHz. In RACS and the VAST pilot survey, discoveries include a number of GRB afterglow candidates (Leung et al. 2021, 2023), highly variable sources near the Galactic Center including candidate Galactic Center Radio Transients (Wang et al. 2022), radio counterparts to known classical novae (Gulati et al. 2023),

Corresponding author: Yuyang Chen
yuyangf.chen@mail.utoronto.ca

¹ We use the term “slow” to differentiate transients that evolve over days to years from unique populations of fast radio transients that have durations of milliseconds to seconds, such as fast radio bursts (e.g., see Pietka et al. 2015)

numerous minute-timescale variable and transient radio sources (Wang et al. 2023), flaring radio stars (Pritchard et al. 2024), a sample of radio-classified TDEs (Dykaar et al. 2024), radio counterparts to optically-discovered TDEs (Anumarlapudi et al. 2024), and a number of SNe with re-brightening radio counterparts at late times (Rose et al. 2024).

The Low Frequency Array (LOFAR; van Haarlem et al. 2013) has been conducting surveys such as the LOFAR Two-metre Sky Survey (LoTSS Shimwell et al. 2017, 2019, 2022) at 144 MHz and the LOFAR Low Band Antenna Sky Survey (LoLSS de Gasperin et al. 2021, 2023) at 54 MHz. Searches of LoTSS have yielded an upper limit on the density of transients with a timescale of $\sim 2\text{--}9$ yr (de Ruiter et al. 2021) and one minute-timescale transient source (de Ruiter et al. 2023).

The Karl G. Jansky Very Large Array (VLA; Perley et al. 2011) has previously conducted the Caltech-NRAO Stripe 82 Survey (CNSS; Mooley et al. 2016) at 3.0 GHz over the ~ 270 deg² Stripe 82 region during 2012–2014. The CNSS was a survey dedicated to transient search and led to discoveries such as stellar flares (Mooley et al. 2016), the first radio-discovered TDE (Anderson et al. 2020), and active galactic nuclei (AGNs) that transitioned from radio-quiet to radio-loud (Mooley et al. 2016; Kunert-Bajraszewska et al. 2020; Wołowska et al. 2021).

Over 2017–2024, the VLA has been conducting the VLA Sky Survey (VLASS; Lacy et al. 2020) at 3.0 GHz over the entire sky North of -40° declination. The complete VLASS includes three epochs separated by ~ 1000 d, and is therefore ideal for detecting slow radio transients that evolve over years to decades. Transient searches in VLASS are actively ongoing, and studies so far have showcased promising results. In VLASS, individually reported discoveries include a decades-long off-axis GRB afterglow (Law et al. 2018; Marcote et al. 2019; Mooley et al. 2022), the first known merger-triggered SN (Dong et al. 2021), an emerging pulsar wind nebula harboring a highly magnetized decades-old neutron star (Dong & Hallinan 2023), and a number of TDE candidates (Ravi et al. 2022; Somalwar et al. 2022) including possibly the first radio-selected relativistic TDE (Somalwar et al. 2023b). Systematic searches of VLASS have also revealed populations of AGNs and galaxies that transitioned from radio-quiet to radio-loud (Nyland et al. 2020; Zhang et al. 2022), long-lasting radio counterparts of a number of SNe (Stroh et al. 2021), a sample of radio-selected TDEs that tends to have properties differing from optically-selected TDEs (Somalwar et al. 2023c,a,d), and a sample of solar-type stars that display transient or variable radio emission (Davis et al. 2024). Additionally, a commensal instrument on the VLA – the VLA Low-band Ionosphere and Transient Experiment (VLITE; Clarke et al. 2016; Polisensky et al. 2016) – has been conducting the VLITE Commensal Sky Survey (VCSS; Peters et al. 2021) simultaneously with

VLASS at 340 MHz. In VCSS, three radio flares have been detected from hot magnetic stars (Polisensky et al. 2023).

Evidently, these surveys provide an unprecedented view of the dynamic radio sky. However, radio surveys themselves provide limited information. In addition to the discovery, extensive follow-up observations are most often required to characterize the properties of a radio-identified transient. For example, targeted multi-band radio observations are usually necessary for extracting the radio spectral energy distribution (SED) and for understanding the emission mechanism (such as the characteristic broken power law profile representing a synchrotron spectrum; Sari et al. 1998; Granot & Sari 2002), and optical imaging and spectroscopy are often crucial for classification and host association (also important for distance determination in many cases).

Since follow-up observations require a range of additional resources, they cannot be performed for every transient and are typically dedicated to the most unique and scientifically interesting discoveries. As a result, the selection of transients worthy of follow-up is an important step for a systematic search. Such selection usually revolves around specific properties. Some simple and effective approaches adopted in the literature involve selecting transients based on brightness (e.g., the extraordinarily bright relativistic TDE candidate discovered by Somalwar et al. 2023b), timescale (e.g., the decades-long off-axis GRB afterglow discovered by Law et al. 2018), or specific classifications of interest (e.g., AGNs that appear as radio transients, as discovered by Nyland et al. 2020).

In principle, the spectral index α is another property that can be useful for this selection process, which characterizes the steepness of a power law spectrum (we adopt the definition $S_\nu \propto \nu^\alpha$ for a power law throughout this study). Certain types of radio sources are known to have distinctive distributions of spectral index. For example, pulsars are known to have steep negative spectral indices ($\alpha \sim -1.6$; Jankowski et al. 2018) while certain blazars and X-ray binaries are known to produce relatively flat radio spectra ($\alpha \sim 0$; Padovani 2016; Hjellming & Johnston 1988). Therefore, spectral index information can be useful for classification schemes and the selection of specific types of objects (e.g., Riggi et al. 2024).

Certain properties may also be inferred from spectral indices. In particular, a positive spectral index ($\alpha > 0$) can be an indication of absorption (Rybicki & Lightman 1979), including synchrotron self-absorption (SSA) and free-free absorption (FFA). In the radio, a spectrum with a positive spectral index is sometimes referred to as an inverted spectrum because the typical spectral index of radio sources is negative (e.g., see spectral index distributions derived from VLASS; Gordon et al. 2021). An inverted spectrum places lower limits on the peak/turnover frequency and flux density, and

constrains physical properties such as the emission size (Kellermann & Pauliny-Toth 1981), which, for an expanding outflow (assuming negligible external absorption), restricts the dynamical age (i.e., a high-frequency peak implies a small size and a young dynamical age). This concept has been used to argue for the youth of some compact radio-loud AGNs that have inverted spectra below some \sim GHz spectral peak (under the assumption of SSA; Shklovsky 1965; Snellen et al. 1998; An & Baan 2012). The same concept applies to transients that in many cases produce radio emission through an expanding shock. In particular, for radio synchrotron transients, the peak frequency is expected to continuously decline and the spectral index (at \sim GHz frequency) should transition from a steep positive value (such as $\alpha = 2.5$ for SSA) to a steep negative value ($\alpha \sim -1.0$) as the transient ages and becomes optically thin (Sari et al. 1998; Granot & Sari 2002). Consequently, an inverted spectrum for a transient could also imply some degree of youth. Therefore, a positive spectral index (or an inverted spectrum) can be useful for constraining physical properties during the selection of transients and is potentially a viable criterion for selecting dynamically young transients.

In practice, spectral information has not always been accessible from radio surveys. Usually, spectral indices are derived from comparing different surveys at different frequencies taken at different times, which are inaccurate for transient sources due to spectral evolution. In many of the new generation radio surveys, in-band spectral information will be provided as part of the data products (Shimwell et al. 2017; Lacy et al. 2020; McConnell et al. 2020), which will undoubtedly be beneficial for studying transients. However, in-band information has some limitations such as limited spectral coverage, large uncertainty, and the need for additional data processing resulting in delay in its release. Currently, useful spectral information is still largely unavailable in released catalogs from ongoing radio surveys. At the moment, none of the reported systematic transient searches in ongoing radio surveys make use of spectral information during the selection process.

A viable way of deriving spectral index of a transient is still through multi-band flux measurements, and requiring the measurements be taken (at least quasi-) simultaneously. There are two ongoing surveys well-suited for this task – VLASS and VCSS – which scan the sky simultaneously at 3.0 GHz and 340 MHz, respectively. The order of magnitude separation in frequency provides significant leverage for characterizing the spectral slope of the radio continuum, and simultaneity ensures that the derived spectral indices are accurate for transient sources. Therefore, transient searches that combine VLASS and VCSS can incorporate spectral index and in theory, take advantage of the supplementary constraints encoded within this quantity.

In this study, we present our search for transients with inverted spectra ($\alpha > 0$) in epoch 1 of VLASS and VCSS. Considering the depth and cadence, these two surveys are excellent for finding bright, slow-evolving, extragalactic transients. Our primary objective is to determine whether it is feasible to discover and select interesting transients based on spectral index and to broadly evaluate the types of transients and physical constraints that result from such searches, particularly in VLASS and VCSS. In essence, this is a proof-of-concept study aimed to gauge expectations for transient selections that incorporate spectral information, which is a concept mostly unexplored in the current literature. Ideally, the results of our study can serve as inspiration for future transient searches as spectral information become more widely available from radio surveys (either from in-band spectrum or simultaneous multi-band measurements).

This study is structured as follows. In Section 2, we describe the radio surveys used and the method of our search for inverted-spectra transients. In Section 3, we present our final sample of transient candidates along with our findings regarding multi-wavelength counterparts. In Section 4, we discuss possible classifications for our transient candidates, examine the physical constraints associated with the inverted spectra, and reflect on the feasibility of our search method. Finally, we summarize and conclude our study in Section 5. Throughout this study, we assume a flat universe with $H_0 = 67.4 \text{ km s}^{-1} \text{ Mpc}^{-1}$ and $\Omega_m = 0.315$ (Planck Collaboration et al. 2020).

2. METHODS

2.1. Description of Radio Surveys

VLASS (Lacy et al. 2020) is a recent survey with the VLA that began in September 2017. VLASS covers the entire sky North of -40° declination ($\sim 82\%$ or $33,885 \text{ deg}^2$ of the sky) in the 3.0 GHz (2.0–4.0 GHz) band over each observing epoch with an angular resolution of 2.5 arcsec. VLASS was designed to have three observing epochs, each separated by $\sim 1000 \text{ d}$, to be completed in October 2024. For this study, we utilize the VLASS component catalogs produced by the Canadian Initiative for Radio Astronomy Data Analysis² (CIRADA; Gordon et al. 2021) using VLASS quick look (QL) images³. Specifically, we use the epoch 1 catalog with 3,347,423 components (version 3) for the transient search and we also use the epoch 2 catalog (version

² See <https://cirada.ca/vlasscatalogueql0>.

³ QL images are rapidly-processed images generated from a relatively simple imaging algorithm with some known quality issues in flux density and astrometry (Lacy et al. 2022b).

Table 1. General Information on Relevant Radio Surveys

Survey	Frequency (MHz)	Sky Overlap (deg ²)	Epoch	Resolution (arcsec)	Image rms (mJy/beam)	Match Radius (arcsec)
VLASS Epoch 1 & 2	3000	...	2017–2022	2.5	0.14	...
VCSS Epoch 1 & 2	340	29800	2017–2022	20	3.0	5
RACS-low	888	23300	2019–2020	25	0.3	5
RACS-mid	1368	28900	2020–2022	10	0.2	3
LoTSS DR2	144	5700	2014–2020	6	0.08	2
NVSS	1400	33880	1993–1996	45	0.45	5
FIRST	1400	10800	1993–2004, 2009–2011	5	0.15	3
WENSS	325	10000	1990s	54	3.6	5
TGSS	150	31500	2010–2012	25	3.5	5
AT20G	4800, 8640, 20000	13000	2004–2008	10	10	4

NOTE—The sky overlap is the survey area overlapping with VLASS crudely estimated using HEALPix (Górski et al. 2005). Note that although some surveys are ongoing, we only list the epochs of the data used in this study. The match radius is for cross-matching with the VLASS catalogue, chosen based on the astrometric uncertainty of the survey. See Section 2.1 for references.

2) to examine variability. The median rms of the QL images is $\sim 140 \mu\text{Jy}/\text{beam}$.

VCSS (Peters et al. 2021) is a survey conducted simultaneously with VLASS by VLITE, a commensal instrument on the VLA developed jointly by the U.S. Naval Research Laboratory and the NRAO (Clarke et al. 2016; Polisensky et al. 2016). VCSS images are processed through the VLITE Database Pipeline (Polisensky et al. 2019). VCSS covers the same regions of the sky as VLASS in the 340 MHz (320–384 MHz) band (although with a wider field of view at lower frequency) with an angular resolution of 20 arcsec. However, we note that the VCSS sky coverage has some empty regions or holes because VLITE was offline or imaging was unfeasible due to insufficient data or nearby bright sources (see Peters et al. 2022). For the transient search, we utilize the VCSS epoch 1 catalog with 573,293 components generated using the Python Blob Detector and Source Finder (PyBDSF; Mohan & Rafferty 2015). The median rms of the VCSS epoch 1 images is $\sim 3 \text{ mJy}/\text{beam}$.

In addition to VLASS and VCSS, we make use of available catalogs and images from past radio surveys, including the NRAO VLA Sky Survey (NVSS; Condon et al. 1998), the Faint Images of the Radio Sky at Twenty-Centimeters (FIRST; Becker et al. 1995) survey, the Westerbork Northern Sky Survey (WENSS; Rengelink et al. 1997), the TIFR Giant Metrewave Radio Telescope Sky Survey Alternative Data Release (TGSS; Intema et al. 2017), and the Australia Telescope 20 GHz (AT20G; Murphy et al. 2010) survey. We use these past surveys as templates for the transient search, particularly NVSS and TGSS which have similar sky cover-

age, resolution, and sensitivity as VLASS and VCSS, respectively. Past surveys that only partially overlap with VLASS and VCSS (WENSS, FIRST, and AT20G) are used for additional confirmation.

Lastly, after obtaining a list of transient candidates, we also search three recent surveys, RACS data release (DR) 1 in the lowest band (RACS-low; McConnell et al. 2020; Hale et al. 2021), RACS in the mid band (RACS-mid Duchesne et al. 2023b,a), and LoTSS DR2 (Shimwell et al. 2022). These surveys were carried out at times near epoch 1 and 2 of VLASS but at lower frequencies, which we utilize to confirm detections and obtain further spectral coverage. Table 1 outlines some general information regarding the radio surveys described above.

2.2. Search for Inverted-Spectra Transients

The goal of our search is to obtain a list of transient candidates in epoch 1 of VLASS and VCSS with inverted spectra. Our general strategy involves identifying transient candidates through comparing VLASS with past radio surveys, and identifying candidates with inverted spectra through comparing VLASS with VCSS. We use a number of selection criteria to ensure that our final list of candidates is robust. The steps of our search are described below and the number of remaining sources after each step is listed in Table 2.

1. Reduce Contamination in VLASS:

Image artifacts can easily be misidentified as transients. To minimize contamination from artifacts, we follow the recommendations of the CIRADA cat-

alog User Guide (July 26, 2023 version)⁴ and select components from the VLASS epoch 1 catalog with $Quality_flag = 0|4|8|12$, $P_sidelobe < 0.05$, $S_Code \neq E$, and $Duplicate_flag < 2$. The resulting sample from this selection has an estimated contamination (i.e., number of real sources over number of artifacts) of only $\sim 0.12\%$. This sample is then used in the following steps.

2. Compact VLASS Sources:

Considering the cadence of VLASS (~ 1000 days) and the brightness threshold of inverted-spectra sources (lower limit set by VCSS $5\sigma \sim 15$ mJy; see step 3 below), we expect to mainly find bright extragalactic synchrotron transients (Pietka et al. 2015). Based on the light travel time argument, sources at extragalactic distances that vary in brightness over multiple years should be compact in VLASS⁵. Therefore, we first identify compact VLASS sources for the transient search.

We define a compactness criterion following the method described by de Ruiter et al. (2021) and Shimwell et al. (2019) to identify compact sources. First, we construct a parameter space, shown in Figure 1, consisting of the ratio of total flux density to peak flux density (S_{tot}/S_{peak}) and the ratio of peak flux density to local noise (S_{peak}/rms). We then select a sample of predefined compact sources in VLASS that satisfy the following conditions: (i) $S_Code = S$, i.e., well fit by a single Gaussian, (ii) total flux density greater than 3 mJy to ensure completeness, (iii) nearest neighboring source more than 45 arcsec away (twice the combined beam size of VLASS and VCSS), and (iv) major axis smaller than 5 arcsec. We divide the predefined compact sources into ten bins over S_{peak}/rms , and for each bin, we find the S_{tot}/S_{peak} value that is above 95% of the predefined compact sources in the bin. Finally, we fit the 95% levels with the function

$$\frac{S_{tot}}{S_{peak}} = \text{offset} + A \cdot \left(\frac{S_{peak}}{rms} \right)^B, \quad (1)$$

where the offset is defined to be the median plus three times the median absolute deviation of S_{tot}/S_{peak} of the predefined compact sources with $S_{peak}/rms > 1000$. We find the best-fit parameters to be $A = 11.48$, $B = -0.76$, and $\text{offset} = 1.10$. We define all VLASS sources below this function in the parameter space to be compact sources (i.e., all points below the black dashed line in Figure 1).

⁴ https://ws.cadc-ccda.hia-ihp.nrc-cnrc.gc.ca/files/vault/cirada/tutorials/CIRADA_VLASS_catalogue_documentation_2023_june.pdf

⁵ A source that is variable over $t \sim 10$ yr with emission size ct will only be resolved if it is at a distance of $\lesssim 250$ kpc given the resolution of VLASS of 2.5 arcsec.

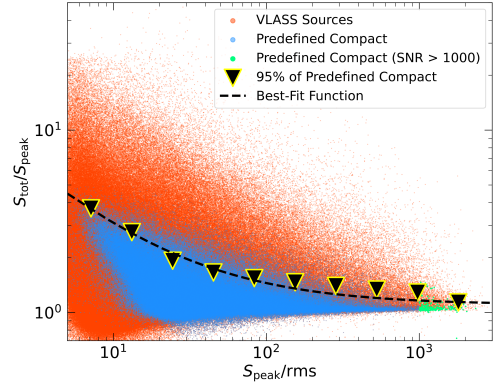


Figure 1. Total flux density over peak flux density versus peak flux density over local noise for VLASS sources (red points). Blue points represent the predefined compact sample and green points represent those with $SNR > 1000$. The black triangles enclose 95% of the blue points within each bin. The dashed line is the best-fit envelope from fitting the black triangles. All points below the dashed line are defined to be compact VLASS sources.

3. Inverted Spectra in VLASS and VCSS

In this step, we cross-match the compact VLASS epoch 1 sources with the VCSS epoch 1 catalog to identify compact sources with inverted spectra. Considering the astrometric uncertainty of VLASS and VCSS, we use a match radius of 5 arcsec. Additionally, to exclude empty regions of the VCSS sky coverage from our search, we remove VLASS sources that have no neighboring VCSS sources within 15 arcmin. From matching, we obtain two populations: (i) sources detected by both VLASS and VCSS and (ii) sources detected by VLASS but not VCSS. Note that we do not consider sources detected by VCSS but not VLASS because these would not have inverted spectra.

Before estimating spectral index, we apply flux density corrections to the catalogs, as both VLASS QL and VCSS catalogs are known to have underestimated flux densities (Lacy et al. 2022b; Peters et al. 2022). For the VLASS epoch 1 catalog, following the analysis in Appendix A, for epoch 1.1 and 1.2, we apply a correction factor of 1/0.95 and 1/0.98 to the total flux densities and add an additional 7% and 3% of the total flux densities in quadrature to the uncertainty, respectively. For the VCSS epoch 1 catalog, we apply the correction function⁶ shown in Figure 2 of Peters et al. (2022).

We use the corrected total flux densities to estimate spectral indices. For sources detected in both VLASS

⁶ The correction is in the form of $S_{obs}/S_{corr} = ae^{-b \cdot SNR} + c$ where $a = -0.382$, $b = 0.032$, $c = 0.899$ for total flux density and SNR is the signal-to-noise ratio.

and VCSS, we directly calculate their spectral indices between 340 MHz and 3.0 GHz⁷ assuming $S_\nu \propto \nu^\alpha$, where S_ν is the total flux density and α is the spectral index. Errors of the indices, σ_α , are estimated from propagating the flux density errors. For sources detected in VLASS but not VCSS, we assume an upper limit of $S_{340\text{MHz}} < 15$ mJy, corresponding to the average 5σ level of VCSS, and estimate a lower limit on α .

Finally, we identify sources with inverted spectra by selecting those with $\alpha > 0$. For sources detected in both VLASS and VCSS, we select those with $\alpha - 3\sigma_\alpha > 0$. For sources detected in VLASS but not VCSS, we select those with $S_{3.0\text{GHz}} - 3\sigma_{S_{3.0\text{GHz}}} > 0$, where $\sigma_{S_{3.0\text{GHz}}}$ is the error of the flux density in VLASS. Note that limited by the sensitivity of VCSS, $S_{3.0\text{GHz}} \gtrsim 15$ mJy is required for $\alpha > 0$, which implies a detection level of $\gtrsim 100\sigma$ in VLASS. Therefore, VLASS sources selected from this step are highly unlikely to be random noise structures.

4. Identifying Potential Transients

After selecting compact VLASS sources with inverted spectra, we then identify the transient candidates in this sample. For this study, we consider a transient to be a source detected in VLASS at 3 GHz that was not detected in past radio surveys listed in Table 1. The most relevant comparison is with NVSS, which has the closest frequency (1.4 GHz), identical sky coverage, and adequate depth (typical 5σ upper limit of ~ 2.3 mJy). This definition of a transient is pragmatic and is designed to capture sources displaying significant variability likely associated with transient phenomena.

In this step, we cross-match the compact inverted-spectra VLASS sources with the NVSS, FIRST, TGSS, WENSS, and AT20G catalogs (using the match radii listed in Table 1 chosen based on astrometric uncertainties of the surveys) and exclude all sources with a match. Remaining sources without a match would then be potential inverted-spectra transients.

5. Removing Known Active Galactic Nuclei

AGNs are known to manifest as variable radio sources and are not considered traditionally as transient sources (Barvainis et al. 2005). Thus, variable AGNs are not a target of interest in this study. In an attempt to reduce AGN ‘‘contamination’’, we remove known/cataloged AGNs by cross-matching our sample with the Wide-field Infrared Survey Explorer (WISE) R90 AGN catalog (Assef et al. 2018), the Sloan Digital Sky Survey

⁷ Note that we assume the VLASS flux density to be at 3.0 GHz but technically, it is over a band of 2.0–4.0 GHz with a large fractional bandwidth. This introduces a small error of less than 5% in the flux density for a power law spectrum with α between -1.0 and 2.0, which should not significantly impact our analysis.

(SDSS) Quasar catalog (DR16Q_v4; Lyke et al. 2020), and the Milliquas catalog (v8; Flesch 2019, 2021, 2023). We exclude all sources with a match within a radius of 3.3 arcsec following the finding of D’Abrusco et al. (2013). This step should be effective in removing bright AGNs that dominate the emission at optical and infrared (IR) wavelengths. However, it does not exclude AGNs with faint optical and IR emission or AGNs too distant to be reliably classified. Therefore, in the following sections, we will still consider the possibility that our final sample may contain AGNs, particularly those that are presumably weaker or heavily absorbed and have then brightened significantly in the radio (see Section 4.1.4).

6. Visual Inspection

In this last step, we visually inspect the survey images of the remaining sources for a final check and reject sources that we consider to be false positives (such as artifacts or persistent sources) misidentified as transients. Generally, we find false positives to be caused by (i) resolution difference between surveys, (ii) outliers with relatively large astrometric uncertainty, or (iii) degraded local image quality in past surveys.

Due to the resolution difference between VLASS and NVSS (2.5 arcsec versus 45 arcsec), we often find false positives when multiple neighboring VLASS sources are blended into a single NVSS source. In this case, the centroid of the blended NVSS source can be significantly offset from the VLASS position, meaning that the VLASS source will not be matched to the NVSS source within our chosen radius of 5 arcsec. As a result, the VLASS source is misidentified as a potential transient, which we reject as a false positive. Also, we find that this issue exists for all remaining sources that have neighboring VLASS sources within 45 arcsec (resolution of NVSS). For future searches, it may be possible to reduce the impact of resolution difference by introducing an additional step of rejecting sources that are not isolated (e.g., reject sources with a neighbor within the beam size of the lower resolution survey).

Occasionally, for isolated VLASS sources, we still see a nearby NVSS source at ~ 5 – 10 arcsec, slightly farther away than our chosen match radius of 5 arcsec. While in theory, it is possible that these are two transients – a disappearing NVSS source and an appearing VLASS source – coincidentally nearby, a more likely explanation is that the two sources are associated but have relatively large astrometric uncertainties, especially considering the scattering in the astrometry of VLASS (Figure 8 of Gordon et al. 2021) and NVSS (Figure 28 and 29 of Condon et al. 1998). Therefore, to ensure that our final candidates are robust, we also reject these sources as false positives.

We typically find degraded NVSS image quality in the Galactic plane near extremely bright emission, where local flux density can fluctuate by tens of mJy over large

Table 2. Number of VLASS Sources Remaining After Each Step of Transient Search

Step	Remaining VLASS Sources	VCSS Detection	VCSS Non-detection
1. Reduce Contamination	1,660,228
2. Compact Sources	1,440,639
3. Inverted Spectra	14,628	1,320	13,308
4. Potential Transients	1,460	1	1,459
5. Removing AGNs	1,190	1	1,189
6. Visual Inspection	22	1	21

NOTE—The last two columns show the number of VLASS sources detected and not detected in VCSS.

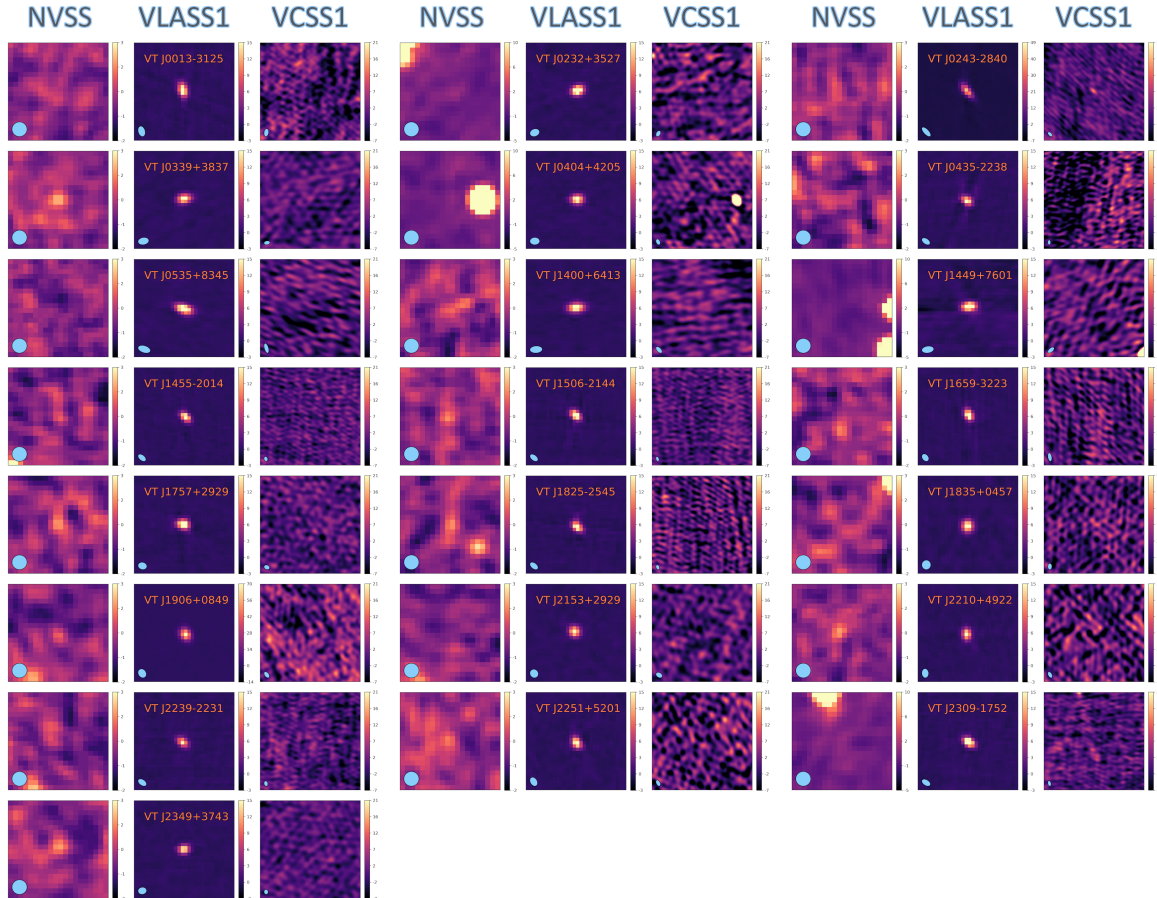


Figure 2. Radio cutout images centered at the locations of the inverted-spectra transient candidates from NVSS, VLASS epoch 1 (VLASS1), and VCSS epoch 1 (VCSS1), arranged into three columns. The names of the candidates are shown in the VLASS1 images. The image size (side length) is 5 arcmin, 30 arcsec, and 5 arcmin for NVSS, VLASS1, and VCSS1, respectively. For each image, the synthesized radio beam (blue ellipse) is shown at the lower left and a colorbar (in mJy) is shown on the right side.

spatial scales. In this case, a non-detection in NVSS can only provide a shallow limit, often exceeding the measured VLASS flux density of $\gtrsim 15$ mJy, which cannot be used as evidence of significant variability between NVSS and VLASS. Therefore, we reject sources in regions with degraded NVSS image quality as false positives.

After rejecting the false positives described above, the remaining sources are considered to be real transient candidates. Ultimately, we found 22 inverted-spectra transient candidates from our search procedure. Figure 2 shows cutout images of the candidates from NVSS, VLASS epoch 1, and VCSS epoch 1.

3. RESULTS

Our search resulted in a sample of 22 transient candidates with inverted spectra (between 340 MHz and 3.0 GHz) in epoch 1 of VLASS and VCSS, with one detected and 21 not detected in VCSS. After the search, for temporal coverage, we obtained measurements for the candidates from epoch 2 of VLASS and VCSS (note that some candidates lack VCSS epoch 2 measurements since they fall on the empty regions of the VCSS epoch 2 sky coverage). For more comparison and spectral coverage, we also searched RACS-low, RACS-mid, and LoTSS DR2 using match radii listed in Table 1. However, we do not use RACS or LoTSS for deriving spectral indices because their observations are not taken at the same time as VLASS and VCSS.

Table 3 contains the collected radio properties of our transient candidates, including names, positions, observing times, radio flux densities, and VLASS-VCSS spectral indices. We follow previous studies and adopt the letters VT (VLASS Transient) for names. Note that the tabulated flux density upper limits are 3σ limits where σ is the local rms calculated using a box centered at the locations of the candidates. The box size (side length) is chosen to be 120 arcsec, 120 arcsec, 30 arcsec, 150 arcsec, 90 arcsec, and 90 arcsec for NVSS, VCSS, VLASS, RACS-low, RACS-mid, and LoTSS DR2, respectively, to capture local noise and avoid nearby sources. The tabulated lower limits of α are also calculated using the local 3σ flux density limits. We also show optical cutout images at the locations of the candidates in Figure 3 (details discussed in Section 3.1.2 and 3.1.3).

It is interesting to note that (as far as we are aware in the literature) none of our transient candidates have been reported by recent searches of ongoing radio surveys except for VT J0243-2840. The discovery of VT J0243-2840 was previously reported by Somalwar et al. (2023b), which resulted from two independent searches: one search compared VLASS and NVSS (similar to the procedure described by Dong & Hallinan 2023) and the other was our search for inverted-spectra transients (i.e., this study). We are also aware that VT 1906+0849 has been discovered separately with extensive follow-up observations that will be reported in

a future study (J. Miller et al., in prep.). Nonetheless, we appear to have found a new sample of transient candidates, which already hints the potential of transient discovery in radio surveys and inverted spectra as a selection criteria. In this section, we examine the properties of our transient candidates in detail. In particular, we discuss our search for multi-wavelength counterparts (Section 3.1) and the general radio properties of the candidates (Section 3.2).

3.1. Multi-wavelength Counterpart and Classification

3.1.1. Searching for Archival Transient Counterparts

For our inverted-spectra transient candidates, we searched the Transient Name Server⁸, the Open Supernova Catalog⁹ (Guillochon et al. 2017), and the Open TDE Catalog¹⁰ for potential archival transient counterparts, particularly SNe and TDEs, before or after the VLASS observations. We found no matches within 1 arcmin of our candidates.

We also searched the GRBweb¹¹, which contains GRBs retrieved from GCN-circulars¹², Fermi Gamma-ray Burst Monitor catalog (von Kienlin et al. 2020), Fermi Large Area Telescope (Atwood et al. 2009), Swift (Gehrels et al. 2004), interplanetary network¹³, BepoSAX catalog (Boella et al. 1997), and the Burst And Transient Source Experiment catalog (Paciesas et al. 1999). Against well-localized GRBs with a 1σ position error of $\lesssim 1$ arcsec, we found matches to be at least separated by 0.4 deg ($\gtrsim 1000\sigma$). Against GRBs with 1σ position error < 1 deg, we found no significant matches, as all but one of our transient candidates are outside the error circles by at least 3σ . Only VT J0232+3527 is within the 2.8σ error circle of GRB 920721D that has a fairly large 1σ position error of 0.73 deg. Against GRBs with poorer localizations (1σ position error ≥ 1 deg and < 10 deg), we found that every one of our transient candidates are matched to dozens of GRBs within their 2σ error circle. Therefore, we cannot reliably claim that any of the GRB matches are real associations.

3.1.2. Searching for Cataloged Optical Galaxy and Stellar Counterparts

We searched for galaxy counterparts in the Panoramic Survey Telescope and Rapid Response System 1 (PS1; Chambers et al. 2016) Source Types and Redshifts with Machine Learning catalog (PS1-STRM; Beck et al. 2021), the Dark Energy Spectroscopic Instrument (DESI) Legacy Imaging Surveys DR8 photometric

⁸ <https://www.wis-tns.org/>

⁹ <https://sne.space/>

¹⁰ <https://tde.space/>

¹¹ <https://user-web.icecube.wisc.edu/~grbweb-public/>

¹² <https://gcn.nasa.gov/circulars>

¹³ <https://www.mpe.mpg.de/~jcg/grbgen.html>

Table 3. Radio Measurements of the VLASS-VCSS Epoch 1 Inverted-Spectra Transient Candidates

Name	R.A.	Decl.	MJD	$S_{1.4\text{GHz}}$	MJD	$S_{3.0\text{GHz}}$	$S_{340\text{MHz}}$	α	MJD	$S_{3.0\text{GHz}}$
	(J2000)	(J2000)	(NVSS)	(NVSS)	(Epoch 1)	(VLASS1)	(VCSS1)	(Epoch 1)	(Epoch 2)	(VLASS2)
	(deg)	(deg)	(d)	(mJy)	(d)	(mJy)	(mJy)		(d)	(mJy)
VT J0013-3125	3.27815	-31.41743	49269	<1.3	58665.5	20.5±0.7	<9.5	>0.35	59625.9	19.8±0.6
VT J0232+3527	38.07406	35.46137	49336	<1.7	58645.5	22.6±0.7	<11.5	>0.31	59523.4	25.6±0.8
VT J0243-2840	40.94038	-28.67775	49250	<1.6	58166.1	53.8±3.6	31.4±4.5	0.25±0.07	59154.2	59.2±1.8
VT J0339+3837	54.84758	38.63292	49336	<2.6	58586.7	17.8±0.6	<7.2	>0.42	59546.3	14.4±0.5
VT J0404+4205	61.22167	42.08469	49336	<3.6	58617.7	18.8±0.6	<11.8	>0.21	59511.5	15.7±0.5
VT J0435-2238	68.86741	-22.64586	49250	<1.8	58161.0	19.2±1.3	<17.2	>0.05	59149.4	19.8±0.7
VT J0535+8345	83.79209	83.76150	49280	<1.5	58074.2	23.7±1.6	<11.5	>0.33	59104.3	27.4±0.8
VT J1400+6413	210.00266	64.21716	49314	<2.0	58084.5	20.4±1.4	<11.1	>0.28	59080.0	19.0±0.6
VT J1449+7601	222.32510	76.01997	49280	<1.8	58056.0	23.2±1.7	<10.5	>0.36	59095.1	<0.6
VT J1455-2014	223.77882	-20.24222	50238	<1.5	58162.5	22.0±1.5	<6.4	>0.57	59147.8	26.0±0.9
VT J1506-2144	226.68930	-21.74295	50238	<1.9	58162.5	25.1±1.7	<7.5	>0.55	59147.8	14.9±0.5
VT J1659-3223	254.86653	-32.39264	49735	<1.8	58153.6	22.9±1.6	<12.3	>0.29	59173.8	19.9±0.7
VT J1757+2929	269.38016	29.49229	49823	<2.3	58028.1	26.0±1.7	<7.9	>0.54	59103.2	30.5±1.0
VT J1825-2545	276.45508	-25.75572	50238	<2.3	58166.6	24.9±1.7	<10.8	>0.38	59146.9	24.2±0.9
VT J1835+0457	278.91964	4.95932	49775	<1.7	58559.6	17.9±0.6	<11.8	>0.19	59485.1	20.2±0.7
VT J1906+0849	286.57567	8.82469	50268	<1.7	58053.1	76.6±5.1	<13.1	>0.81	59092.0	37.5±1.3
VT J2153+2929	328.49995	29.49528	49853	<1.2	58625.4	17.6±0.6	<9.4	>0.29	59489.3	21.4±0.7
VT J2210+4922	332.57300	49.37413	49793	<2.1	58626.5	17.1±0.6	<15.2	>0.06	59505.3	13.8±0.5
VT J2239-2231	339.88860	-22.52422	49250	<1.9	58665.4	17.3±0.6	<7.1	>0.41	59625.8	15.5±0.6
VT J2251+5201	342.92041	52.03047	49788	<2.4	58626.5	19.3±0.6	<13.2	>0.18	59514.3	18.4±0.6
VT J2309-1752	347.42478	-17.88210	49250	<2.2	58670.5	27.3±0.9	<9.1	>0.51	59614.8	18.1±0.7
VT J2349+3743	357.33369	37.72596	49835	<2.3	58593.6	16.9±0.5	<5.8	>0.50	59510.3	14.5±0.5

$S_{340\text{MHz}}$	α	MJD	$S_{888\text{MHz}}$	MJD	$S_{1368\text{MHz}}$	MJD	$S_{150\text{MHz}}$	Spectrum
(VCSS2)	(Epoch 2)	(RACS-low)	(RACS-low)	(RACS-mid)	(RACS-mid)	(LoTSS DR2)	(LoTSS DR2)	
(mJy)		(d)	(mJy)	(d)	(mJy)	(d)	(mJy)	
<15.0	>0.13	58936.1	<1.0	59220.4	2.0±0.3	Highly Inverted
<13.4	>0.30	58594.3	2.3±0.7	59207.5	8.1±0.9	58420.8	3.1±0.2	Highly Inverted*
19.2±6.3	0.52±0.15	58601.2	45.8±3.7	59210.5	65.1±3.9	Peaked
<7.4	>0.30	58594.3	15.2±1.6	59207.5	13.4±0.9	Peaked
<12.1	>0.12	59206.6	4.5±0.4	Highly Inverted
<9.5	>0.34	58599.5	<1.0	59237.6	2.7±0.3	Highly Inverted
<7.7	>0.58
<8.7	>0.36	58773.3	0.8±0.2	Highly Inverted
<10.8
<8.4	>0.52	58600.6	<0.6	59424.4	2.0±0.3	Highly Inverted
<9.0	>0.23	58934.8	<0.8	59276.8	3.2±0.4	Highly Inverted
<9.1	>0.36	58601.9	3.0±0.9	59231.1	7.2±0.5	Highly Inverted
<8.6	>0.58	58594.8	<0.9	59218.1	3.5±0.4	58697.7	1.4±0.4	Highly Inverted*
<9.5	>0.43	59020.6	4.2±1.0	59231.1	8.8±0.6	Highly Inverted
<10.3	>0.31	58971.8	<0.8	59238.1	<0.6	Highly Inverted
...	...	58972.9	52.3±4.4	59236.2	40.9±2.5	Peaked
<12.8	>0.24	58598.0	<0.9	59216.3	2.3±0.4	58758.7	<0.5	Highly Inverted
<7.6	>0.27
...	...	58601.1	9.1±1.3	59208.4	16.5±1.0	Peaked
<11.1	>0.23
...	...	58601.1	11.1±1.4	59235.3	16.4±1.0	Peaked
<5.5	>0.44	58595.1	3.1±0.7	59209.4	8.9±0.7	Highly Inverted

NOTE—The symbol < and > indicates upper limit and lower limit, respectively. Note that flux density upper limits are 3σ where σ is the local rms. Values after the \pm symbol are 1σ errors. The spectral index α is calculated using only $S_{3.0\text{GHz}}$ and $S_{340\text{MHz}}$. The final column indicates the rough spectral shape if measurements at different frequencies are connected, and * is marked if additional complexity is present in the spectrum (see Section 3.2.1 for details).

redshift catalog (Duncan 2022), SDSS DR18 (Almeida et al. 2023), and the Galaxy List for the Advanced Detector Era + catalog (Dállya et al. 2022). We found nine transient candidates to be within $\sim 0.1\text{--}0.3$ arcsec of galaxies with photometric redshift estimates spanning $z_{\text{phot}} \sim 0.1 - 1.0$, shown in Table 4. We consider these to be real matches because of the small separations. In the PS1-STRM catalog, the matched counterparts (those with z_{phot}) have high probabilities of being galaxies ($P \gtrsim 0.89 - 0.99$) and not quasars, which is reassuring given that we have removed bright optically-selected AGNs. In the optical images, extended emission associated with galaxies can be seen (Figure 3) and the small separations from the radio positions suggest that the transient candidates could reside in the nuclei of the matched galaxies.

In Table 4, we also provide the derived (isotropic) spectral luminosity (L_ν) and time between epoch 1 and 2 in the frame of the galaxy ($\Delta t/(1+z_{\text{phot}})$). Note that we adopted z_{phot} with the smallest error when there are estimates from multiple catalogs. We did not propagate the redshift error to L_ν and we have not applied a k-correction (e.g., the factor of $(1+z)^{-(1+\alpha)}$ for a power law) due to our lack of knowledge on the exact spectral shape and the precise value of α . Therefore, the derived L_ν should be treated as order-of-magnitude estimates over the *observed* frequency range of 2.0–4.0 GHz that could be slightly overestimated. The error of $\Delta t/(1+z_{\text{phot}})$ is propagated from z_{phot} . At the estimated redshifts, the spectral luminosities of our transient candidates are $L_\nu \sim 10^{30} - 10^{33} \text{ erg s}^{-1} \text{ Hz}^{-1}$.

We note that five of our candidates are within the SDSS footprint, but only the counterpart of VT 0535+8345 was detected by SDSS, and with no spectrum. The counterpart of VT 0243-2840 has been observed by the 2dF Galaxy Redshift Survey (2dFGRS; Colless et al. 2001) with a recorded spectroscopic redshift of $z = 0.07$, which is the same value as the estimated photometric redshift. The 2dFGRS spectrum of VT 0243-2840 has been analyzed in detail by Somalwar et al. (2023b), along with a newer optical spectrum. Thus, we do not perform any analysis on existing optical spectra of VT 0243-2840 and we simply reference the results of Somalwar et al. (2023b) in relevant discussions.

We also searched for possible stellar counterparts in Gaia DR3 (Gaia Collaboration et al. 2016, 2023) but found no counterparts for candidates that are not matched to galaxies. Also, counterparts in the PS1-STRM catalogs have low probabilities of being stars. Therefore, our transient candidates do not appear to be associated with known or obvious optical stellar sources in the Milky Way.

3.1.3. Searching for Additional Infrared, X-ray, and Optical Counterparts

We searched for IR counterparts in the Wide-field Infrared Survey Explorer (WISE; Wright et al. 2010) catalogs – AllWISE (Cutri et al. 2021), unWISE (Schlafly et al. 2019), and CatWISE (Marocco et al. 2021). WISE magnitudes of 11 for our transient candidates from cross-matching with AllWISE (using a match radius of 1.5 arcsec) are shown in Table 5, which we use for later analyses regarding possible classifications (Section 4.1). None of these AllWISE matches were flagged for significant variability ($var_flg = 0$ for 10 candidates and $var_flg = 3$ for one candidate). We note that for a few candidates (VT J1506-2144, VT J1757+2929, and VT J2210+4922), we found AllWISE matches within $\sim 1.5\text{--}3.0$ arcsec, but we do not use these for our analyses because of possible issues from crowding and blending of nearby emission as seen in the images. Additionally, three of our candidates (VT J0339+3837, VT J1835+0457, and VT J1906+0849) with no counterparts in AllWISE have relatively faint counterparts in unWISE or CatWISE.

We searched for X-ray counterparts in the Chandra Source Catalog Release 2.0 (Evans et al. 2010), the XMM-Newton Serendipitous Source Catalog DR13 (Webb et al. 2020), the Swift-XRT Point Source Catalog (Evans et al. 2020, 2023) and the eROSITA-DE DR1 catalogs (v1.1 for Main and v1.0 for Hard; Merloni et al. 2024). We found an X-ray counterpart for VT J0232+3527 observed by Chandra (Obs ID 7111) with a reported X-ray flux of $F_{0.5\text{--}7.0\text{keV}} \sim 2 \times 10^{-14} \text{ erg s}^{-1} \text{ cm}^{-2}$. We also found X-ray observations for VT J0243-2840 observed by Swift (obsid 00014300001 and 00014364003) and XMM-Newton (Obs. ID 0872393201) obtained by Somalwar et al. (2023b) specifically for this radio transient candidate. Somalwar et al. (2023b) reported an X-ray flux of $F_{0.3\text{--}10\text{keV}} \sim 10^{-13} \text{ erg s}^{-1} \text{ cm}^{-2}$ (corresponding to $L_{0.3\text{--}10\text{keV}} \sim 10^{42} \text{ erg s}^{-1}$) with a soft photon index of $\Gamma_X \sim 3$ and a negligible intrinsic column density. Note that based on the data archives, most of our other transient candidates have never been in any observing fields of Chandra, XMM-Newton, or Swift-XRT.

In eROSITA-DE DR1, only five of our transient candidates (VT J0243-2840, VT J0435-2238, VT J1455-2014, VT J1506-2144, VT J1659-3223) are within the covered hemisphere, and only VT J0243-2840 was detected at $F_{0.2\text{--}2.3\text{keV}} \sim 10^{-13} \text{ erg s}^{-1} \text{ cm}^{-2}$ (confirming the soft spectrum). For those not detected in eROSITA-DE, we found 3σ upper limits¹⁴ to be $F_{0.2\text{--}2.3\text{keV}} \lesssim (4 - 9) \times 10^{-14} \text{ erg s}^{-1} \text{ cm}^{-2}$. For VT J0435-2238, which has a photometric redshift estimate, the upper limit translates to $L_{0.2\text{--}2.3\text{keV}} \lesssim 10^{42} \text{ erg s}^{-1}$. Overall, we found fairly few X-ray constraints for our transient candidates.

¹⁴ Accessed through <https://erosita.mpe.mpg.de/dr1/erodat/upperlimit/single/>. Details of the upper limits are described by Tubín-Arenas et al. (2024).

Table 4. Photometric Redshifts and and Derived Properties

Name	z_{phot}	$L_{\nu, \text{Epoch1}}$ ($10^{31} \text{ erg s}^{-1} \text{ Hz}^{-1}$)	$L_{\nu, \text{Epoch2}}$ ($10^{31} \text{ erg s}^{-1} \text{ Hz}^{-1}$)	$\Delta t / (1 + z_{\text{phot}})$ (d)
VT J0013-3125	0.58±0.02	29.94	28.93	607.8±7.7
VT J0243-2840	0.07±0.006	0.69	0.76	923.5±5.2
VT J0435-2238	0.28±0.03	5.08	5.23	772.1±18.1
VT J0535+8345	0.15±0.005	1.55	1.79	895.8±3.9
VT J1400+6413	1.06±0.11	130.65	121.7	483.3±25.8
VT J1757+2929	0.48±0.08	24.13	28.32	726.4±39.3
VT J2210+4922	0.08±0.004	0.29	0.23	813.7±3.0
VT J2239-2231	0.14±0.008	0.98	0.87	842.4±5.9
VT J2309-1752	0.09±0.011	0.59	0.39	866.4±8.7

NOTE—Values after the \pm symbol are 1σ errors.

For transient candidates that are not matched to galaxy counterparts, we searched the PS1 survey (Chambers et al. 2016) and the DESI Legacy Surveys DR10 (Dey et al. 2019) for unclassified optical counterparts (see Figure 3 for cutout optical images). Note for one candidate at low declination (VT 1659-3223) that is not within the coverage of PS1 and Legacy Survey DR10, we instead searched Gaia DR3 and the SkyMapper Southern Sky Survey (SMSS) DR2 (Onken et al. 2019). Also note that we only consider counterparts separated by <1 arcsec from the radio positions (similar to the VLASS astrometric uncertainty; Gordon et al. 2021). From this search, we found three candidates (VT J0232+3527, VT J1506-2144, and J1906+0849) with faint and red optical counterparts, which leaves five candidates (VT J0404+4205, VT J1449+7601, VT J1659-3223, VT J1825-2545, and VT J2251+5201) with no optical or IR counterparts.

Finally, we checked the Zwicky Transient Facility public DR19 (Bellm et al. 2019; Masci et al. 2019) and the Asteroid Terrestrial-impact Last Alert System forced photometry (Tonry et al. 2018; Smith et al. 2020; Shingles et al. 2021) for optical light curves at the location of our transient candidates. We found no evidence of variability in the optical light curves for any candidate.

3.2. General Radio Properties

3.2.1. Spectral Energy Distributions

In Figure 4, we show crude radio SEDs of our inverted-spectra transient candidates using flux density measurements and upper limits from Table 3. We show a power law through the VLASS and VCSS measurements with a shaded error region for the one candidate detected in both surveys. For the other 21 cases with no VCSS de-

tections, we show a shaded region that spans the range from a shallow power law with the lower limit of α (through the VCSS upper limit) to a steep power law with $\alpha = 2.5$, the expected spectral index for SSA (in a homogeneous environment).

In our search for potential transients, non-detection in NVSS was considered a primary indicator of significant variability. As shown in the radio SEDs, connecting the VLASS detection with the NVSS non-detection would require $\alpha \gtrsim 2.5$, which would be highly unusual for persistent radio sources (e.g., very few compact VLASS sources have $\alpha > 2$ as seen by Gordon et al. 2021). The natural explanation would be variability between NVSS and VLASS, which is confirmed by the RACS-mid *detections* all being brighter than the NVSS 3σ upper limits. However, there may still be a possibility that we have selected variable radio sources with highly inverted spectra, which we also discuss below.

The crude radio SEDs with measurements at different frequencies provide rough depictions of the spectral shape if we assume that our transient candidates evolve slowly at the observed frequencies (which is likely a reasonable assumption based on the two epochs of VLASS; see Section 3.2.2). Broadly, we notice two types of spectral shape over $\nu \sim 0.8 - 3.0$ GHz: (i) highly inverted spectra and (ii) peaked spectra. The highly inverted spectra are seen with an approximate slope of $\alpha \sim 2.0 - 3.0$ connecting the VLASS and RACS measurements (e.g., VT J0013-3125). On the other hand, the peaked spectra show RACS measurements comparable to the VLASS measurements and above the VCSS measurements/limits (e.g., VT J0243-2840), indicating a turnover/peak near the observed frequencies ($\nu_{\text{peak}} \lesssim 1 - 3$ GHz). In the final column of Table 3, we list the broad spectral shape for each transient candidate. Overall, these spectra are consistent with the ex-

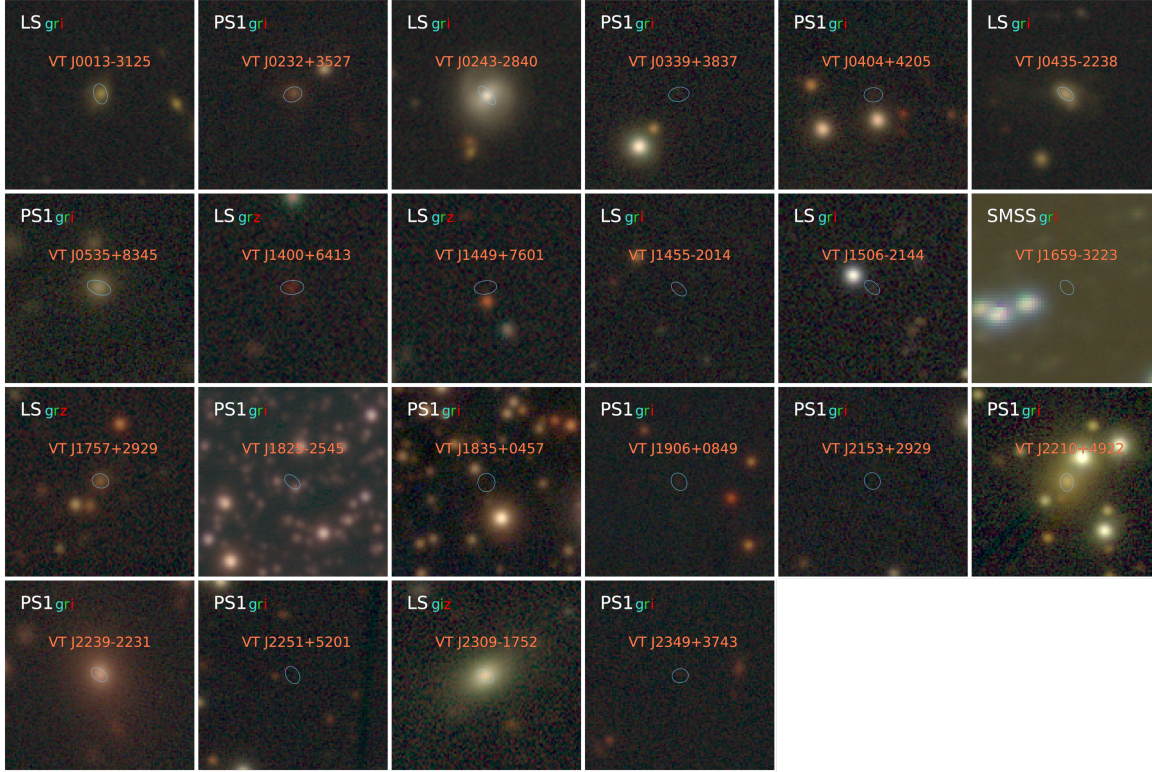


Figure 3. Three-color optical cutout images (30×30 arcsec) of the inverted-spectra transient candidates from Legacy Survey (LS) DR10, PS1, or SMSS DR2. A combination of the *griz* bands, depending on availability, are used to for the three colors. The names and the synthesized radio beam (blue ellipse) of the candidates are shown in each image.

Table 5. AllWISE Magnitudes of Transient Candidates

Name	W1 (mag)	W2 (mag)	W3 (mag)	W4 (mag)
VT J0013-3125	15.94 ± 0.05	15.55 ± 0.11	>12.25	>8.94
VT J0232+3527	14.49 ± 0.03	13.93 ± 0.04	11.37 ± 0.17	>8.18
VT J0243-2840	14.14 ± 0.03	14.03 ± 0.03	10.60 ± 0.07	7.68 ± 0.18
VT J0435-2238	15.24 ± 0.03	14.77 ± 0.06	11.53 ± 0.17	>8.60
VT J0535+8345	14.10 ± 0.03	13.51 ± 0.03	11.09 ± 0.12	8.59 ± 0.30
VT J1400+6413	16.03 ± 0.04	15.72 ± 0.08	>13.07	>9.31
VT J1455-2014	16.83 ± 0.11	16.57 ± 0.38	12.44 ± 0.43	>8.97
VT J2153+2929	17.78 ± 0.19	>17.55	>12.17	>8.76
VT J2239-2231	13.35 ± 0.03	13.15 ± 0.03	12.04 ± 0.29	>8.32
VT J2309-1752	14.02 ± 0.03	13.78 ± 0.04	10.48 ± 0.09	8.06 ± 0.24
VT J2349+3743	16.44 ± 0.07	15.92 ± 0.14	>12.19	>8.93

NOTE—Magnitudes are in the Vega system. Values after the \pm symbol are 1σ errors. The $>$ sign indicates upper limit magnitude.

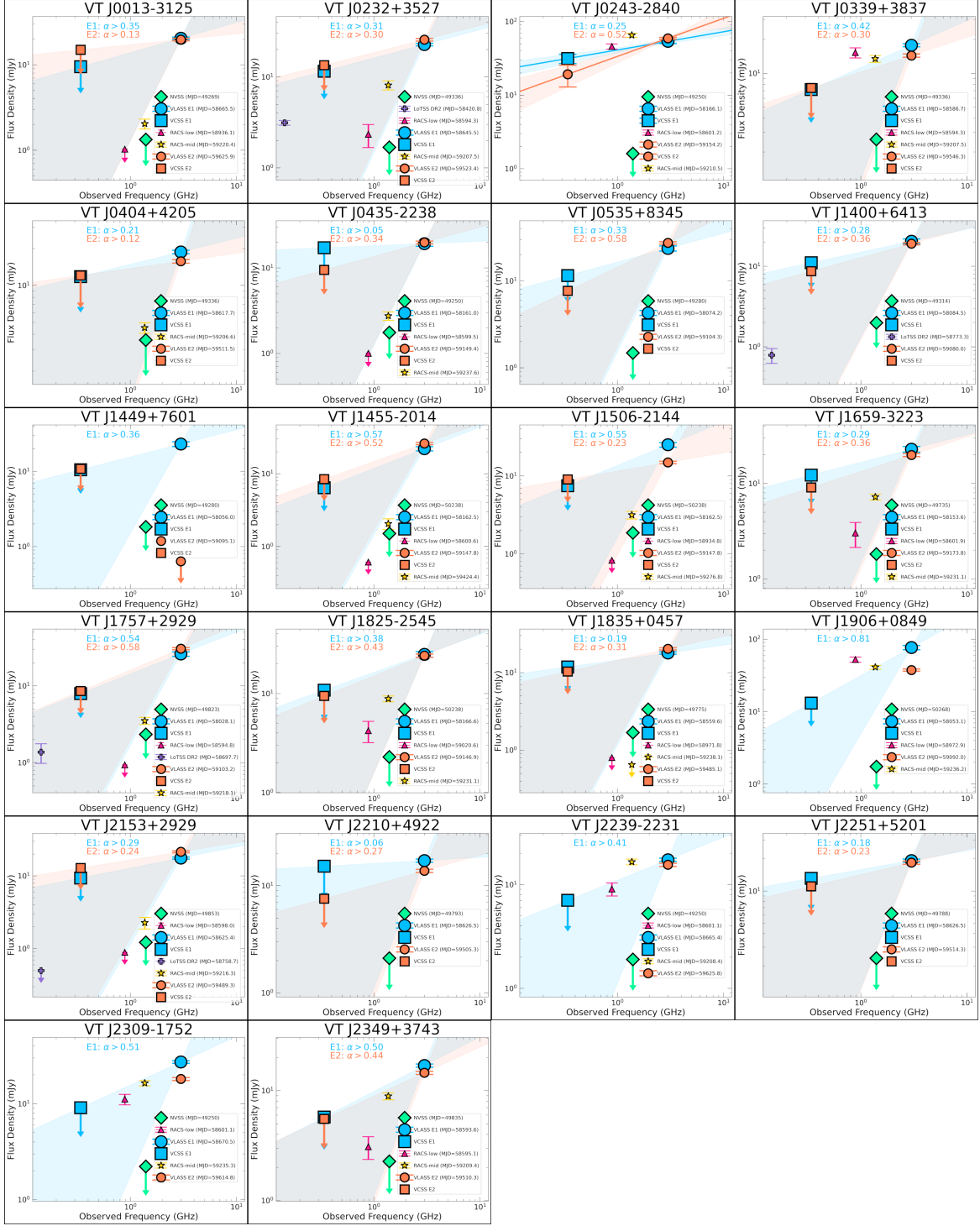


Figure 4. Radio SEDs of the inverted-spectra transient candidates using measurements from NVSS, VLASS, VCSS, RACS-low, and LoTSS DR2 (see Table 3). Names of the candidates are shown as the plot titles. Spectral indices α from epoch 1 (E1) and epoch 2 (E2) are also shown at the top. Downward arrows below the points indicate (3σ) upper limits. Legend labels are ordered from top to bottom by increasing epoch. If the candidate is detected in both VLASS and VCSS, a power law with a shaded error region is shown. If the VCSS measurement is an upper limit, then the shaded region spans the range from a shallow power law with the lower limit α (through the upper limit of VCSS) to a steep power law with $\alpha = 2.5$.

pected synchrotron spectra of transients that are highly inverted at low frequency and turn over at high frequency (Sari et al. 1998). In this context, the difference between the observed highly inverted spectra and peaked spectra is the location of the spectral peak, i.e., the former suggests a spectral peak beyond the observed frequencies ($\nu_{\text{peak}} \gtrsim 3$ GHz). The exact location of the spectral peak depends on various physical parameters, which we discuss in Section 4.2.

For a few of our transient candidates, we also notice two unusual characteristics or complexities in their radio SEDs. The first is the LoTSS detections of VT J0232+3527 and VT J1757+2929, which are brighter than the RACS-low measurements, possibly revealing excess emission at low frequency on top of the inverted spectrum (power law) traced by RACS. An explanation for such excess could be a different spectral component at low frequency (e.g., a power law with $\alpha < 0$ at $\lesssim 800$ MHz), perhaps associated with persistent radio emission from the host galaxy (e.g., Callingham et al. 2017) or a separate low-frequency transient component. Due to limited spectral and temporal coverage, the exact characteristics (e.g., spectral shape) and origin of the low-frequency emission is currently unclear. Nonetheless, it is intriguing to note that since two out of four LoTSS measurements reveal a low-frequency spectrum more complex than a simple power law, we may speculate that such complexity could be common among our transient candidates.

The other unusual characteristic is the extremely inverted ($\alpha \gtrsim 4.0$) spectrum between RACS and VLASS seen in VT J1835+0457. In particular, the RACS-mid non-detection for VT J1835+0457 is fully consistent with the NVSS non-detection, meaning that we have no evidence of significant variability over the past few decades for this source. Therefore, rather than a radio transient with an optically thick $\alpha > 2.5$ spectrum (which can happen, e.g., due to external FFA; Sfaradi et al. 2023), it is entirely possible that VT J1835+0457 is a persistent source, i.e., a rare case of a radio-loud AGN with an extremely inverted spectrum (e.g., Callingham et al. 2015). In addition to this source, we also note that a number of our transient candidates have RACS-mid flux densities that are only slightly brighter than the NVSS 3σ upper limits. These candidates could perhaps also be explained by radio-loud AGNs with highly inverted spectra ($\alpha > 2.5$) that were below the depth of NVSS but brightened moderately prior to RACS-mid at 1.4 GHz. The existence of such sources certainly raises the concern that our sample of transient candidates may still be “contaminated” by variable AGNs that have unusually inverted spectra. We discuss this possibility in more detail in Section 4.1.4 and consider it as a caveat of our method in Section 4.3.

Finally, we note that with the exception of VT J1449+7601, all of our transient candidates have been detected in the two epochs of VLASS and many

are detected in other radio surveys at different frequencies over several epochs. We consider these detections to be strong evidence that our transient candidates are real objects and not imaging artifacts. For the particular case of VT J1449+7601 (only detected in VLASS epoch 1), we find that it is ~ 3 arcmin away from a relatively bright source (at ~ 0.25 Jy). While the faint sidelobes of the bright source are visible at the location of VT J1449+7601, the signal-to-noise ratio of VT J1449+7601 is still very high at $\gtrsim 60$. There are also two other sources at tens of mJy near this bright source that are detected in both epoch 1 and 2 of VLASS. However, because of its vicinity to a bright source, we cannot rule out the possibility that VT J1449+7601 is an artifact from image construction or the CLEAN process. Thus, we caution that VT J1449+7601 is the least reliable detection in our sample of transient candidates.

3.2.2. Radio Variability in VLASS

With flux density measurements from epoch 1 and 2 of VLASS, we calculated the variability of our inverted-spectra transient candidates, shown in Figure 5. The majority of our candidates show $\lesssim 20\%$ variability in VLASS between epoch 1 and 2. Any brightening of the candidates were $\lesssim 20\%$ while the fading of some candidates reached $\sim 20\text{--}60\%$. One candidate (VT J1449+7601) showed significant fading of $>97\%$ (bottom right outlier in Figure 5) as it was not detected in epoch 2 (although there is ambiguity as to whether the first detection was real, as mentioned in Section 3.2.1). We note that only nine candidates show $>3\sigma$ variability, and that the variability of the other 13 candidates is not statistically significant. Overall, if these candidates are real transients, our results imply that we may be selecting sources that evolve very slowly over years to decades.

However, with two data points, it is ambiguous whether any variation between the two epochs occurred smoothly or sporadically. While changes in brightness are expected to follow some power law for a simple synchrotron transient (Granot & Sari 2002), irregular variation can also arise due to episodic flaring or extrinsic scattering (e.g., Bannister et al. 2016). Hence, the characteristic of the light curve is useful information that is reflective of the nature of the transient. For multi-epoch sampling, we checked ASKAP surveys (as of Mar. 15, 2024) and found light curves (with more than two data points) for VT J0243-2840, VT J1455-2014, and VT J1825-2545 from a combination of RACS, VAST, the First Large Absorption Survey in HI (FLASH; Alison et al. 2022), and the Widefield ASKAP L-band Legacy All-sky Blind survey (WALLABY; Koribalski et al. 2020). The light curves are shown in Figure 6. For these three transient candidates, there is some gradual brightening over years at a frequency lower than 3.0 GHz (of VLASS), and we see no significant indication of any sporadic variation or multiple peaks beyond the mea-

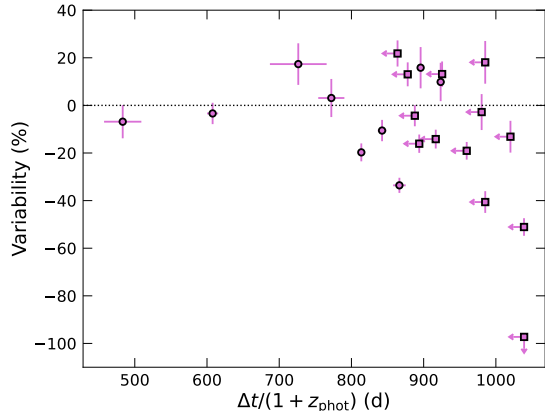


Figure 5. Variability of the inverted-spectra transient candidates in VLASS, defined as the percentage change in $S_{3.0\text{GHz}}$ between epoch 1 and 2, plotted against the change in time $\Delta t/(1 + z_{\text{phot}})$. Calculated $\Delta t/(1 + z_{\text{phot}})$ values are shown as circles and upper limits (due to the lack of redshift estimates) are shown as squares.

surement uncertainties. The only notable feature is the apparent narrow peak at the end of the VT J0243-2840 light curve, but it is hard to interpret due to large uncertainty. The overall smooth brightening is consistent with a synchrotron transient that predicts brightening at the inverted portion of the spectrum until the spectral peak moves below the observing frequency (Granot & Sari 2002; Metzger et al. 2015). At the moment, with no evidence of sporadic changes or multiple flares, slow evolution is still the simplest explanation for the marginal level (or even the lack) of variability of our transient candidates.

4. DISCUSSION

We have selected a sample of 22 inverted-spectra transient candidates in epoch 1 of VLASS and VCSS and have compiled flux density measurements from recent radio surveys at different frequencies over similar epochs. Furthermore, we searched for counterparts in the optical, IR, and X-ray, and obtained photometric redshift estimates for a number of our candidates. In this section, we combine our findings and consider possible classifications of our transient candidates (Section 4.1), examine physical constraints encoded within the inverted spectra (Section 4.2), and reflect on the feasibility of our search method (Section 4.3).

4.1. Considerations on Classifications

Based on the radio brightness/luminosity, timescale, spectral characteristics, as well as multi-wavelength associations, we can make some evidence-based speculations regarding the possible classifications of our transient candidates. For this exercise, the luminosity and timescale turn out to be two particularly useful pieces of information. Therefore, to begin, we show in Figure 7

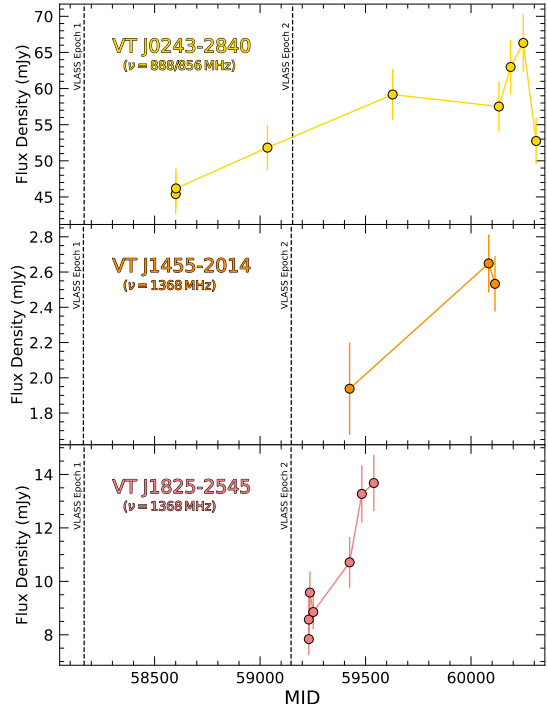


Figure 6. Light curves of transient candidates with more than two data points at a similar frequency from ASKAP surveys RACS, VAST, FLASH, and WALLABY (see text for references). Frequency is shown below the Name. Dashed vertical lines mark the times of VLASS epoch 1 and 2. Note that the errors are conservative estimates that add in quadrature the cataloged flux density error, the image rms, and a systematic error of 6%.

the radio spectral luminosity light curves of our transient candidates (with a common arbitrary start time), and refer to it in relevant discussions below.

4.1.1. Non-Relativistic Extragalactic Transients

For our transient candidates with estimated photometric redshifts, the derived spectral luminosities span the range of $L_\nu \sim 10^{30} - 10^{33} \text{ erg s}^{-1} \text{ Hz}^{-1}$ (Figure 7). This level of brightness immediately disfavors supernovae (SNe) that have $L_\nu \lesssim 10^{29} \text{ erg s}^{-1} \text{ Hz}^{-1}$ over $\nu \sim 4 - 10 \text{ GHz}$ (Bietenholz et al. 2021) and luminous fast blue optical transients (LFBOTs) that have $L_\nu \lesssim 10^{30} \text{ erg s}^{-1} \text{ Hz}^{-1}$ at $\nu \lesssim 10 \text{ GHz}$ (Ho et al. 2019; Margutti et al. 2019; Coppejans et al. 2020; Ho et al. 2020; Bright et al. 2022; Ho et al. 2022). Also, SNe and LFBOTs typically evolve and fade significantly over ~ 1000 days at a few GHz, but our transient candidates only showed marginal levels of variability. Based on the brightness, we also disfavor thermal (non-relativistic)

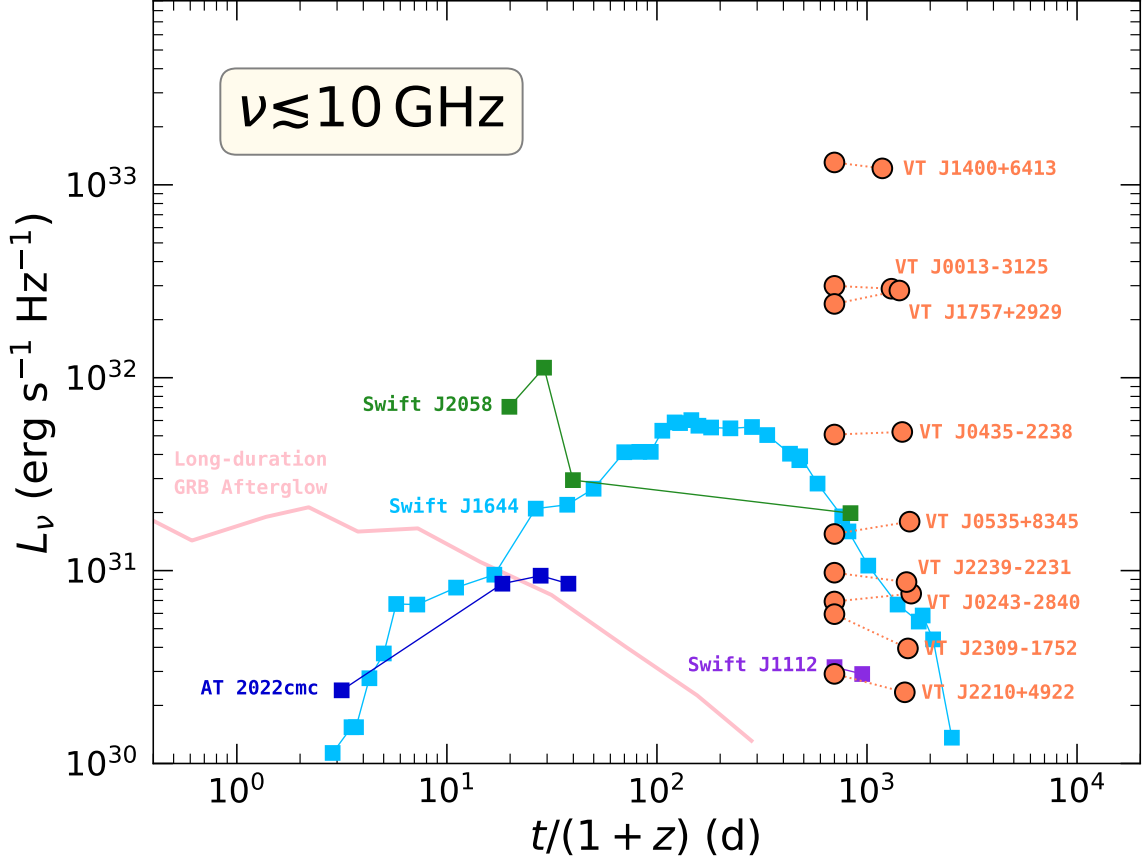


Figure 7. Spectral luminosity light curves (in the frame of the host galaxies) from VLASS epoch 1 and 2 measurements (orange circles at 3.0 GHz) of inverted-spectra transient candidates. Note that an *arbitrary* start time (700 days prior to epoch 1) is set for all of our candidates since the real start times are not known. For comparison, we also show the averaged long-duration GRB afterglow light curve (pink solid line at 8.5 GHz; Chandra & Frail 2012) and light curves of four relativistic TDEs, Swift J1644 (light blue squares at 5 GHz except for last four points being 3 GHz; Berger et al. 2012; Zauderer et al. 2013; Eftekhari et al. 2018; Cendes et al. 2021), Swift J2058 (green squares at 7–9 GHz; Cenko et al. 2012; Pasham et al. 2015; Brown et al. 2017), Swift J1112 (purple squares at 5 GHz; Brown et al. 2017), and AT 2022cmc (dark blue squares at 5 GHz; Andreoni et al. 2022; Rhodes et al. 2023)

TDEs¹⁵ that have $L_\nu \lesssim 10^{30} \text{ erg s}^{-1} \text{ Hz}^{-1}$ at $\nu \lesssim 10 \text{ GHz}$ (e.g., Horesh et al. 2021a; Cendes et al. 2023). Thus, we do not consider non-relativistic extragalactic transients as plausible classifications.

4.1.2. Gamma-Ray Bursts

GRBs are extragalactic relativistic transients that can produce bright radio afterglows with $L_\nu > 10^{30} \text{ erg s}^{-1} \text{ Hz}^{-1}$ (e.g., Chandra & Frail 2012). Although we did not find any reliable GRB associations for our transient candidates (Section 3.1.1), such an association is still possible given the large positional un-

certainities of GRBs and potential cases of off-axis GRBs (e.g., Law et al. 2018). However, there are some inconsistencies between the observed properties of our transient candidates and the expected evolution of GRB afterglows.

For our transient candidates, the persistent spectral luminosity on the level of $L_\nu \sim 10^{30} - 10^{33} \text{ erg s}^{-1} \text{ Hz}^{-1}$ over \sim years to a decade timescale is unusual in the context of GRB afterglows, which typically evolve substantially over days to months (Pietka et al. 2015). For example, the observed averaged long-duration GRB afterglow light curve maintains $L_\nu \sim 10^{31} \text{ erg s}^{-1} \text{ Hz}^{-1}$ only over the first month, and fades by more than an order of magnitude over a few hundred days (Chandra & Frail 2012, also shown Figure 7). Therefore, the light curves of typical long-duration GRB afterglows are generally inconsistent with our transient candidates even if the afterglows were detected in VLASS epoch 1 at an early

¹⁵ We follow the conventional assumption that thermal TDEs produce much fainter radio emission than relativistic TDEs. However, we note that Somalwar et al. (2023c) have recently reported evidence that there may not exist a clear boundary in radio luminosity between thermal and relativistic TDEs.

stage. We note that short-duration GRB afterglows are fainter than long-duration GRB afterglows (Fong et al. 2015), so the same inconsistencies exist.

Also, the radio SEDs of our transient candidates show $\nu_{\text{peak}} \gtrsim \text{GHz}$ for $\gtrsim 3 \text{ yr}$, which is difficult to explain with GRB afterglows that usually peak at much lower frequencies at such late times. As an example, we estimate ν_{peak} using the standard GRB afterglow model by Granot & Sari (2002) that assumes a spherical adiabatic blast wave, and adopt reasonable parameters (e.g., Bloom et al. 2003; Santana et al. 2014; Metzger et al. 2015; Beniamini & van der Horst 2017; Chrimes et al. 2022) of isotropic kinetic energy $E_{\text{K,iso}} = 10^{53} \text{ erg}$, fraction of energy in the electrons $\epsilon_e = 10^{-1}$, fraction of energy in the magnetic field $\epsilon_B = 10^{-4}$, electron power-law index $p = 2.5$, and number density $n = 1 \text{ cm}^{-3}$ for a constant density interstellar medium. Taking $t_{\text{obs}} = 1000 \text{ d}$ (observed time approximately between VLASS epochs) and $z = 0.2$, we find $\nu_{\text{peak}} \approx 222 \text{ MHz}$ at the self-absorption frequency. Therefore, the afterglow model predicts that radio emission probed by VLASS and VCSS should be optically thin with $\alpha < 0$ after $\sim 3 \text{ yr}$, which is inconsistent with the observed inverted spectra of our transient candidates during epoch 2.

In similar fashion, we find discrepancies between our transient candidates and the theoretical predictions of GRB afterglows in VLASS by Metzger et al. (2015). In their simulation, on-axis and off-axis long-duration GRB afterglows in VLASS are virtually all expected to brighten or fade by more than a factor of 2 between two VLASS epochs and only be detectable in a single epoch. Compared to the observed marginal levels of variability between VLASS epochs (Figure 5), this again confirms the inconsistency in the timescale between our candidates and GRB afterglows.

Lastly, we note that for the nine transient candidates matched to galaxies, the offsets between the radio positions and the optical galaxy centers are $\sim 0.1\text{--}0.3 \text{ arcsec}$. Since the majority of the matched galaxies are at $z_{\text{phot}} \lesssim 0.2$, we find a preference for projected offsets of $r_{\text{proj}} \lesssim 0.2 - 0.8 \text{ kpc}$. On the other hand, for long-duration (short-duration) GRBs, roughly $\lesssim 30\%$ ($\lesssim 10\%$) of explosion sites are observed to be within $r_{\text{proj}} \lesssim 0.8 \text{ kpc}$ (e.g., Lyman et al. 2017; Fong et al. 2022). This could be another discrepancy between our transient candidates and GRB afterglows, although we note that this discrepancy is only tentative due to uncertainties in the radio positions and z_{phot} .

In summary, based on the observed persistent brightness and inverted spectra over $\gtrsim 3 \text{ yr}$, we do not consider GRB afterglows as a favorable explanation for our transient candidates. However, we do not fully rule out GRB afterglows, because fine-tuning of explosion parameters (perhaps highly energetic cases similar to those reported by Cenko et al. 2011) and considerations of energy injection (Zhang & Mészáros 2001, 2002; Gao et al. 2013) and late-time non-relativistic evolution (Wygoda et al.

2011; Sironi & Giannios 2013) may lead to afterglow properties similar to our transient candidates. Detailed examination of models and viable parameter space is beyond the scope of this study, especially considering our lack of observational constraints.

4.1.3. Galactic Transients

A number of our transient candidates (not matched to galaxies) lie near the Galactic plane: VT J0404+4205, VT J1659-3223, VT J1825-2545, VT J1835+0457, VT J1906+0849, and VT J2251+5201, with Galactic latitudes of $|b| < 8 \text{ deg}$. VT J1906+0849 in particular has $b = 0.74 \text{ deg}$, perhaps suggesting a Galactic origin. Although extended sources (e.g., resolved Galactic sources) are excluded from our transient search, our selection criteria do not explicitly reject compact Galactic radio transients. Therefore, it is worth considering the possibility that some of our transient candidates are Galactic transients.

Various stellar objects manifest as variable or transient radio sources. However, most slow Galactic radio transients, including stellar flares, X-ray binaries, dwarf novae, and magnetar giant flares, evolve over a typical timescale of hours to weeks (e.g., Güdel 2002; Pietka et al. 2015; Mooley et al. 2016, and references therein), whereas our transient candidates have evolved for $\gtrsim 3 \text{ yr}$ in VLASS. Therefore, from timescale alone, it is unlikely that Galactic radio transients constitute a major fraction of our selected candidates. Detecting such Galactic transients in two epochs of VLASS would imply an extraordinarily long timescale or multiple flaring episodes captured coincidentally in two epochs, both of which should be rare. At least for VT J1825-2545, we see smooth brightening over hundreds of days after VLASS epoch 2 (Figure 6).

The radio brightness of and the lack of bright stellar associations for our transient candidates also place heavy constraints on any Galactic transient interpretation. For example, if radio flares from K- or M-type dwarfs can have $L_\nu \sim 10^{15} \text{ erg s}^{-1} \text{ Hz}^{-1}$ (at $\sim \text{GHz}$; Smith et al. 2005; Mooley et al. 2016), then the flux densities of our transient candidates of $F_\nu \gtrsim 15 \text{ mJy}$ would place the stars at $d \lesssim 7.5 \text{ pc}$. Since the coolest M-type dwarfs are found to have an average r -band absolute magnitude of $M_r \sim 18.5$ (Best et al. 2018; Cifuentes et al. 2020), the lack of bright optical counterparts in PS1 with apparent magnitudes $m_r \lesssim 18.5$ is evidence against radio flares from K- or M-type dwarfs. For brighter radio transients associated with, e.g., CVs, Algol systems, and RS CVn stars that have $L_\nu \lesssim 10^{20} \text{ erg s}^{-1} \text{ Hz}^{-1}$ (Pietka et al. 2015; Mooley et al. 2016), $F_\nu \gtrsim 15 \text{ mJy}$ would require $d \lesssim 2.4 \text{ kpc}$. Out to a distance of 2.4 kpc , the PS1 survey (with limiting r -band magnitude of 23.2) should detect stellar objects down to $M_r \lesssim 11.3$, which include all stars hotter and brighter than M-type dwarfs (Cifuentes et al. 2020), although some non-detections may be explainable by significant

dust extinction at low Galactic latitudes. Overall, the lack of bright optical stellar associations for our transient candidates disfavors many types of Galactic radio transients originating from stars.

If any of our transient candidates are Galactic, they are more likely to be the brightest Galactic radio transients detected at larger distances such that any optical counterpart would be faint or obscured. Bright Galactic radio transients that can produce $L_\nu \gtrsim 10^{20} - 10^{22} \text{ erg s}^{-1} \text{ Hz}^{-1}$ include some classical novae (Chomiuk et al. 2021), X-ray binaries (Merloni et al. 2003; Tetarenko et al. 2016), and magnetar giant flares (Gaensler et al. 2005; Cameron et al. 2005). In particular, some classical novae produce synchrotron emission that can evolve over a timescale of $\gtrsim 1000 \text{ d}$ (Chomiuk et al. 2021), which may explain the observed properties of our transient candidates. Therefore, we cannot rule out rare cases of bright Galactic radio transients for some of our transient candidates not matched to galaxies.

4.1.4. Variable Active Galactic Nuclei

The radio properties of our transient candidates are reminiscent of peaked-spectrum (PS) sources such as gigahertz-peaked spectrum (GPS) sources and high-frequency peakers (HFPs), which are radio-loud AGNs characterized by concave radio spectra peaking at $\nu_{\text{peak}} \sim 0.5 - 5 \text{ GHz}$ and $\nu_{\text{peak}} \gtrsim 5 \text{ GHz}$, respectively (O’Dea 1998; O’Dea & Saikia 2021). PS sources have radio luminosities spanning $L_\nu \sim 10^{31} - 10^{36} \text{ erg s}^{-1} \text{ Hz}^{-1}$ and compact radio linear sizes less than a few kpc, down to a few pc for HFPs (e.g., An & Baan 2012; Patil et al. 2020). From the high-frequency peaks and inverted spectra, PS sources have been interpreted as dynamically young precursors of large-scale Fanaroff-Riley classes of galaxies (An & Baan 2012), jets confined by dense environments (the frustration scenario; van Breugel et al. 1984; Wagner & Bicknell 2011), or “short-lived” episodic events (e.g., activity lasting $\lesssim 10^4 \text{ yr}$ due to radiation pressure instability in the accretion disk; Czerny et al. 2009). The properties of PS sources are broadly similar to those of our transient candidates, and since many of our candidates are matched to the optical centers of galaxies (to within the radio positional uncertainty), a nuclear origin for the radio emission is plausible. Thus, we consider the possibility that we may have selected variable AGNs (or even persistent AGN in the case of VT J1835+0457) instead of transients in the traditional sense (e.g., explosive transients).

Before discussing possible scenarios of AGNs, we first gather some information about classification based on the optical and IR counterparts of our transient candidates. In Figure 8, we show the AllWISE IR color-color diagram constructed using magnitudes from Table 5 as well as regions containing luminous or heavily obscured AGNs. IR counterparts of our transient candidates generally fall outside of the AGN regions,

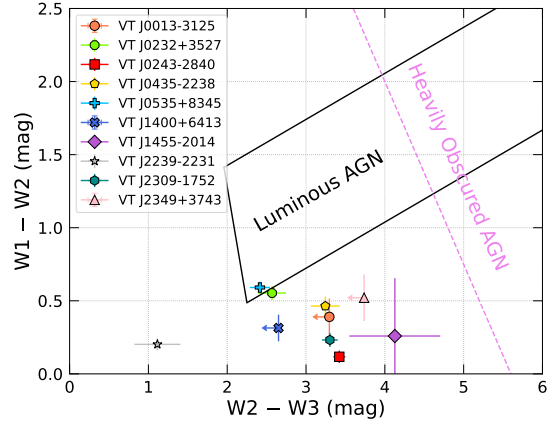


Figure 8. AllWISE color-color diagram for our transient candidates. Upper limits of the W2–W3 color are marked with arrows. The labeled region for luminous AGNs is from Mateos et al. (2012), and the region for heavily obscured AGNs is from Lonsdale et al. (2015) and Patil et al. (2020).

which is expected since we have already removed cataloged AGNs and quasars during our transient search (Section 2.2). The PS1-STRM classifications also indicate that the optical counterparts with photometric redshifts have low probabilities of being quasars. Together with the lack of significant optical and IR variability (Section 3.1), these findings confirm the general exclusion of AGNs with luminous optical and IR emission in our sample. We note two possible exceptions – counterparts of VT J0232+3527 and VT 0535+8345 – that are at the edge of the luminous AGN region. In particular, for VT J0232+3527, PS1-STRM does not report a photometric redshift but does report a high probability for quasar classification.

Ideally, having X-ray information would be beneficial for classification, since X-ray emission is almost ubiquitous in AGNs (Padovani et al. 2017). Unfortunately, we have very limited X-ray constraints for our transient candidates (Section 3.1.3), and existing upper limits do not rule out $L_X \gtrsim 10^{41} - 10^{42} \text{ erg s}^{-1}$ seen in AGNs (Ueda et al. 2014). With the available information, we still cannot rule out weaker AGNs with fainter optical and IR emission and that were previously radio-quiet. For those lacking multi-wavelength information, we also cannot rule out distant AGNs (e.g., higher redshift quasars). In the following discussions, we consider if these types of AGNs can explain our transient candidates.

As noted in Section 3.2.1, there are two broad types of radio SEDs over $\sim 0.3 - 3.0 \text{ GHz}$ seen for our transient candidates – (I) highly inverted SEDs and (II) peaked SEDs. For the most inverted SEDs, the observed differences between NVSS (upper limit) and RACS-mid at 1.4 GHz are small, while for peaked SEDs, significant brightening is seen. Therefore, the required types

of variability are different, so we discuss the two cases separately below.

(I) Highly Inverted SEDs – Moderate Variability

A significant fraction of our transient candidates (7 out of 22) show highly inverted spectra ($\alpha \gtrsim 2.5$) with RACS-mid measurements that are only slightly brighter than the NVSS 3σ upper limits at 1.4 GHz (Figure 4). For these candidates, a possible scenario is that a PS source slightly below the NVSS upper limit experienced moderate brightening of $\gtrsim 20\%$ – 80% prior to VLASS. This scenario may better explain the observed persistent brightness and inverted spectrum over $\gtrsim 3$ yr. There is also a single extreme case of VT J1835+0457 (with $\alpha \gtrsim 4.0$) that shows a RACS-mid upper limit below the NVSS upper limit, meaning that it could be an extremely inverted persistent PS source. We note that the general exclusion of luminous AGNs and quasars does not disfavor PS sources, since many PS sources are classified as galaxies (not quasars) in the optical and IR (Hancock 2009; Kunert-Bajraszewska et al. 2010; Kosmaczewski et al. 2020).

For PS sources, variability is generally low at \sim GHz, at about a few percent over years (O’Dea 1998; Fassnacht & Taylor 2001), but a small fraction of PS sources vary by $\gtrsim 10\%$ – 100% (e.g., Jauncey et al. 2003; Wu et al. 2013; Ross et al. 2021, 2022). On \sim decade timescales, a large fraction of PS sources may show moderate levels of variability (Oriente & Dallacasa 2020). We note that some variable PS sources are known to be misclassified flat-spectrum sources, likely blazars, that show peaked spectra during flares (Tinti et al. 2005; Tornainen et al. 2005; Oriente et al. 2007; Oriente & Dallacasa 2020). However, a flat spectrum below NVSS would imply more than about an order of magnitude brightening at 3 GHz in VLASS, which is much more drastic than typical blazar variability. Therefore, we disfavor blazar variability for our transient candidates.

Intrinsic variability in PS sources may be related to adiabatic expansion or varying optical depth (Oriente et al. 2010; Ross et al. 2022; Oriente & Dallacasa 2020). At 1.4 GHz, the extrinsic effect of refractive interstellar scintillation (strong scattering) can also produce modulation of $m \lesssim 60\%$ over days to months (assuming a critical frequency $\nu_0 \gtrsim 4$ GHz over a range of Galactic latitude; Walker 1998). Another extrinsic effect is an extreme scattering event (ESE), which can lead to irregular variation in the flux density and spectral shape over weeks to months (Bannister et al. 2016). These extrinsic effects may be a possible explanation, but the timing must be correct to produce a non-detection in NVSS and a detection in RACS-mid. Overall, regardless of the exact origin, moderate variability can explain many of our transient candidates with highly inverted radio SEDs *if* we make the assumption that their flux densities were *just below* NVSS and that brightening was captured decades later.

We also note that $\alpha \gtrsim 2.5$ is quite unique for PS sources. Most PS sources have $\alpha \lesssim 1.3$ in the optically thick segment (de Vries et al. 1997; O’Dea 1998; Snellen et al. 1998; Stanghellini et al. 1998; Oriente & Dallacasa 2012; Randall et al. 2012; Callingham et al. 2017), and very few have $\alpha \gtrsim 2.0$. Although steep spectra at low frequencies are expected for homogeneous absorbers, inhomogeneity can result in flatter spectra for both SSA and FFA (e.g., Tingay & de Kool 2003), which is commonly seen in the radio structures of PS sources (O’Dea 1998). In extremely rare occasions, inverted spectra with $\alpha \gtrsim 2.5$ have been found for PS sources, which are generally better described by inhomogeneous FFA rather than SSA (Callingham et al. 2015, 2017; Keim et al. 2019; Mhaskey et al. 2019a,b). Interpretations of these PS sources likely have significant implications on the ambient medium, possibly favoring the frustration scenario for some fraction of radio-loud AGNs (Mukherjee et al. 2016; Bicknell et al. 2018). Also, irregular variability of ESEs can result in highly inverted spectra (Lazio et al. 2001), which we cannot rule out with our limited temporal coverage. We speculate that the extreme case of VT J1835+0457 (with $\alpha \gtrsim 4.0$) may be explained by significant FFA or an ESE if it is a radio-loud AGN.

In the context of PS sources, the apparent overabundance of transient candidates with $\alpha \gtrsim 2.0$ – 3.0 may be a selection effect related to our selection criteria of (i) non-detection in NVSS with $S_{1.4\text{GHz}} \lesssim 2.5$ mJy and (ii) inverted radio spectra with $S_{3.0\text{GHz}} \gtrsim 15$ mJy. Assuming moderate flux density variability over decades but persistent spectral shape, these two criteria will only result in PS sources with highly inverted spectra.

In summary, many of our transient candidates with highly inverted SEDs can be explained by PS sources that show moderate levels of variability (intrinsic or extrinsic) that just happened to produce non-detections in NVSS and brighten during the RACS-mid epoch. However, the highly inverted spectra imply that these PS sources must also be extremely rare, if our transient candidates are even AGNs in the first place. Considering the rarity of such cases, it is unclear at this point whether PS sources are a more favorable explanation over actual transients. If our transient candidates with highly inverted SEDs are variable PS sources, we likely have selected a very peculiar and interesting population of AGNs, although they are persistent sources and not the intended target of this study. Follow-up observations are necessary for distinguishing between AGNs and transients and for constraining the physical origin of the variability, which we leave for future studies.

(II) Peaked SEDs – Extreme Brightening

A considerable number of our transient candidates (9 out of 22) show significant brightening of $\gtrsim 300\%$ – 4000% in RACS-mid at 1.4 GHz compared to NVSS. They have peaked spectra near 1.4–3.0 GHz, but some still show

highly inverted spectra at $\lesssim 0.8\text{--}1.4$ GHz. This observed level of brightening cannot be explained by normal variability of PS sources. In the context of AGNs, these transient candidates are only consistent with recently discovered extreme cases of AGNs that have transitioned from radio-quiet to radio-loud over the past two decades in CNSS (Mooley et al. 2016; Kunert-Bajraszewska et al. 2020; Wołowska et al. 2021) and VLASS (Nyland et al. 2020). The extreme brightening of AGNs in the radio has generally been associated with the launching of young jets possibly from episodic AGN activities, which may signify the birth or rejuvenation of PS sources.

Similarities in radio properties can be found between our transient candidates and the AGNs that experienced extreme brightening. These AGNs were undetected in FIRST and brightened by more than a factor of few, up to more than an order of magnitude in CNSS or VLASS over \sim decade. The radio SEDs of the brightened AGNs were characterized by peaked spectra with $\nu_{\text{peak}} \gtrsim$ GHz that displayed marginal variability over months and years after detection. In general, the radio properties of our transient candidates are very consistent with those of the extreme AGNs.

However, there are some potential uncertainties in associating our transient candidates with extreme AGNs. A significant number of extreme AGNs show $\alpha \lesssim 1.0 - 2.0$ in the optically thick segment (perhaps for the same reason as typical PS sources) while our transient candidates generally show $\alpha \gtrsim 2.0$ between $\lesssim 0.8\text{--}1.4$ GHz, although there is a lack of constraints on α for our SEDs with $\nu_{\text{peak}} \lesssim 1 - 3$ GHz. In terms of galaxy classifications, the VLASS sample of extreme AGNs discovered by Nyland et al. (2020) was selected specifically from cataloged luminous AGNs and quasars, while the CNSS sample discovered by Wołowska et al. (2021) contains both quasars and galaxies. On the other hand, we have explicitly removed luminous AGNs and quasars, and thus galaxies that do not show strong AGN signatures in the optical and IR should constitute a major fraction of our sample of transient candidates.

For the galaxies, Wołowska et al. (2021) assumed that the radio brightening was due to AGN activity and did not consider alternative scenarios such as TDEs. A possible counterexample to this assumption is VT 0243-2840 in our sample, which was examined in detail by Somalwar et al. (2023b). The host galaxy of VT 0243-2840 is a weak Seyfert galaxy, and based on the lack of strong AGN activity, low black hole mass, soft X-ray spectrum, and small radio linear size, Somalwar et al. (2023b) concluded that VT 0243-2840 would be an extremely unusual case if it was caused by AGN activity (although this was not ruled out). On the other hand, Somalwar et al. (2023b) found that a relativistic TDE is a plausible (perhaps more preferable) scenario for VT 0243-2840. We speculate that similar ambiguities may exist for our other transient candidates, so additional con-

straints will be necessary for establishing the origin of the radio brightening in galaxies.

Overall, based on the radio properties, AGNs transitioning from radio-quiet to radio-loud is a plausible explanation for our transient candidates that show significant brightening at 1.4 GHz over \sim decade timescale. However, a major uncertainty lies in the classification of the host galaxy and whether or not there is ongoing AGN activity that can trigger such brightening. Lastly, we remark that phenomenologically, such extreme brightening of AGNs will appear as radio transient objects and thus will be identified in any transient search over \sim decade timescale unless excluded through extensive multi-wavelength constraints. While this may be non-ideal for searches targeting TDEs or explosive transients (which was the original intent of this study), transient AGNs are nonetheless interesting objects that may have important implications on topics including the evolution of radio-loud AGNs, jet launching from supermassive black holes, and the nature of changing-look AGNs (Wołowska et al. 2017; Nyland et al. 2020; Wołowska et al. 2021; Somalwar et al. 2023b).

4.1.5. Relativistic Tidal Disruption Events

Jet launching has been observed in a small subset of TDEs known as relativistic TDEs or jetted TDEs, which generate bright long-lasting radio synchrotron emission as a result of a shock wave propagating through the circumnuclear medium (Alexander et al. 2020). Currently, only a handful of on-axis relativistic TDEs has been discovered in the X-ray and optical, including Swift J1644+57 (Bloom et al. 2011; Burrows et al. 2011; Zauderer et al. 2011), Swift J2058.4+0516 (Cenko et al. 2012), Swift J1112.2-8238 (Brown et al. 2015), and AT 2022cmc (Andreoni et al. 2022). Radio light curves representative of these relativistic TDEs are plotted in Figure 7, showing $L_\nu \sim 10^{30} - 10^{32}$ erg s $^{-1}$ Hz $^{-1}$ and timescales of at least several years. For the most well-studied case, Swift J1644+57, the radio spectral peak was above \gtrsim GHz for the observed period of about 2800 days (or 2060 days in the frame of the host galaxy; Cendes et al. 2021). Therefore, the radio properties of our transient candidates are consistent with observed relativistic TDEs.

We note that on-axis relativistic TDEs are extremely rare, with a volumetric rate of $\mathcal{R} \approx 0.02$ Gpc $^{-3}$ yr $^{-1}$ inferred from the ZTF survey (Andreoni et al. 2022) that is only $\sim 1\%$ of the thermal TDE rate even after a beaming correction (Teboul & Metzger 2023; Yao et al. 2023). Based on this rate, the estimated number of on-axis and off-axis relativistic TDEs in VLASS would be

$$N_{\text{VLASS}} \approx \frac{\mathcal{R} \Delta t \Delta \Omega C}{f_b} \frac{4\pi d^3}{3} \\ \sim 34 \left(\frac{\Delta t}{5 \text{ yr}} \right) \left(\frac{C}{1} \right) \left(\frac{f_b}{0.01} \right)^{-1} \left(\frac{d}{\text{Gpc}} \right)^3, \quad (2)$$

where Δt is the transient duration, $\Delta\Omega \approx 0.82$ is the VLASS sky coverage fraction, C is the completeness of our search, f_b is the beaming factor, and d is the distance. Out to a distance of 1 Gpc (roughly $z=0.2$), we expect roughly a few dozen relativistic TDEs assuming a complete search and reasonable parameters $f_b \sim 0.01$ and $\Delta t \sim 5$ yr. On the other hand, few transient candidates were identified at $z \lesssim 0.2$. The smaller number of observed candidates is not unexpected, because our search is likely incomplete (i.e., $C < 1$) due to additional criteria such as the selection of inverted spectra and exclusion of any host galaxies detectable in NVSS. This comparison implies that rarity does not disfavor the relativistic TDE interpretation for our transient candidates, but also that our sample of candidates does not provide useful constraints on the rate of radio-selected relativistic TDEs (especially when AGNs may exist in our sample).

For the specific candidate VT 0243-2840, Somalwar et al. (2023b) obtained multi-frequency radio follow-up observations and found the radio SEDs to be consistent with an energetic outflow in an ordinary environment (electron density $\gtrsim 1 \text{ cm}^{-3}$) that was mildly relativistic on average ($0.1c < \langle v \rangle < 0.6c$). VT 0243-2840 was interpreted as a candidate relativistic TDE by Somalwar et al. (2023b), and thus would be an example supporting the relativistic TDE interpretation of our transient candidates. We note that there is ambiguity in this case (and likely in all our candidates) that the brightening could be due to some unusual AGN activity (see Section 4.1.4 above). However, at least for our transient candidates that have well-detected optical and IR counterparts (and thus redshift estimates), the lack of strong AGN signatures and variability makes them less likely to be AGNs. Overall, considering the slow-evolving luminous radio emission and the coincidence with galactic nuclei, we argue that the most plausible explanation for our transient candidates is relativistic TDEs (at least for those that lack strong AGN signatures).

We do note, however, that a potential difference between our transient candidates and known relativistic TDEs is the timescale. Compared to relativistic TDEs (mostly the well-studied case of Swift J1644+57) that are seen to vary by a factor of a few over several hundred days, our transient candidates show little variability between the two epochs of VLASS (~ 500 -900 d in the rest frame). It is possible to reconcile this difference if epoch 1 and 2 of VLASS separately captured the rising and fading portions, respectively, but this scenario is unlikely to apply to all candidates. For example, the three candidates that have light curves from ASKAP show relatively smooth brightening over years (Figure 6). According to the simulation by Metzger et al. (2015), only $\sim 50\%$ of TDEs similar to Swift J1644+57 detected in VLASS are expected vary by less than a factor of 2 between two epochs. Therefore, to explain such low levels of variability, our transient candidates likely evolve

much slower than known relativistic TDEs selected in the X-ray and optical.

Somalwar et al. (2023b) similarly remarked on the unusually long timescale of VT 0243-2840, which was brightening for $t/(1+z) \gtrsim 1200$ d (possibly $\gtrsim 3000$ d). VT 0243-2840 also had a break frequency ordering of $\nu_a < \nu_m < \nu_c$ in the most recent radio SED, where ν_a is the self-absorption frequency, ν_m is the characteristic frequency of electrons with minimum energy, and ν_c is the cooling frequency. Such ordering is expected during the earlier phase of the slow cooling scenario and should transition to $\nu_m < \nu_a$ at late times (Granot & Sari 2002), which happened for Swift J1644+57 at $t/(1+z) \gtrsim 222$ d. Somalwar et al. (2023b) suggested that continual energy injection or low energy dissipation may explain the slow evolution.

In summary, we argue that relativistic TDEs are a plausible explanation for our transient candidates, especially if AGN activity can be ruled out in the host galaxies. However, compared to known on-axis relativistic TDEs, our candidates appear to evolve much more slowly over time. The difference in timescale is not necessarily a counterargument against the TDE interpretation, but rather reflects the complexity of TDEs, especially in the radio. Complex behaviors were seen in recent radio observations of thermal TDEs, which showed that a large fraction of optically-selected TDEs experience delayed radio brightening after $t \sim 10^2 - 10^3$ d (Cendes et al. 2023, also see individual cases reported by Horesh et al. 2021a,b; Cendes et al. 2022; Perlman et al. 2022; Goodwin et al. 2023; Christy et al. 2024; Zhang et al. 2024). Proposed explanations for the delayed brightening include delayed outflows (Horesh et al. 2021a; Cendes et al. 2023) and off-axis jets (Matsumoto & Piran 2023; Sfaradi et al. 2024). For relativistic TDEs, some recent theoretical studies have suggested that precession can result in effectively weaker jets that become choked, explaining the rarity of relativistic TDEs, and break out of some choked jets may lead to delayed radio brightening (Teboul & Metzger 2023; Lu et al. 2023). At this point, many open questions exist regarding the exact late-time evolution and behavior of TDEs in the radio, and our candidates may occupy a mostly unexplored slow-evolving regime of relativistic TDEs.

Finally, we note that TDEs studied so far have been almost exclusively selected in the X-ray and optical, but discoveries of radio-selected TDEs will bring forth a different perspective. For example, Somalwar et al. (2023c) recently found tentative trends that radio-selected TDEs have fainter optical emission and prefer galaxies with lower stellar and black hole masses. Dykaar et al. (2024) began constraining volumetric rates of on-axis and off-axis relativistic TDEs through an untargeted search in the VAST pilot survey. Therefore, if (at least some of) our transient candidates are relativistic TDEs, the radio perspective can provide unique insights for the complex processes involved in these rare events. Follow-up ob-

servations and detailed analyses will be crucial for this purpose, which we leave for future works.

4.2. Physical Constraints From Inverted Spectra

The theme of this study is transient selection based on an *inverted spectrum*, motivated by the idea that this spectrum limits the brightness and frequency at the spectral peak and correspondingly constrains specific physical properties. We can now use the observed radio SEDs of our transient candidates to broadly examine the obtainable physical constraints, which will help us better understand what can be expected from a transient search that incorporates inverted spectrum as a selection criterion.

The radio SEDs of our transient candidates roughly constrain the peak frequency¹⁶ to $\nu_{\text{peak}} \gtrsim \text{GHz}$ and the peak luminosity to $L_{\nu, \text{peak}} \gtrsim 10^{30} \text{ erg s}^{-1} \text{ Hz}^{-1}$ given that the VLASS measurements are near or below the spectral peak. We assume the emission to be synchrotron radiation and derive physical quantities that are a function of these two observables following the equipartition analysis of Barniol Duran et al. (2013) and Matsumoto & Piran (2023). Specifically, we calculate the equipartition energy E_{eq} , radius R_{eq} , and ambient electron density n_{ext} for both on-axis (Barniol Duran et al. 2013) and off-axis (Matsumoto & Piran 2023) cases, adopting certain values of the Lorentz factor Γ and viewing angles θ for illustration.

However, because we have very limited observational constraints, we make a number of assumptions for our calculations. These assumptions are (i) equipartition between electrons and magnetic field, (ii) filling factors $f_V = 4/3$ and $f_A = 1$ for the non-relativistic ($\Gamma = 1$) case and $f_V = f_A = 1$ for relativistic ($\Gamma > 1$) cases, (iii) density calculated by $n_{\text{ext}} = N_e / (4\Gamma^2 V)$ where N_e is the number of electrons and $V = f_V \pi R_{\text{eq}}^3 / \Gamma^4$ is the volume, (iv) $\eta = 1$ but no correction to electron energy for $\nu_m < \nu_a$ (essentially ignoring this factor), (v) a redshift $z = 0.2$ (roughly representative of the recorded photometric redshifts), and (vi) bulk of the total energy contained in hot protons leading to a correction factor of $\xi^{1/17}$ and $\xi^{11/17}$ to R_{eq} and E_{eq} , respectively, where $\xi = 1 + \epsilon_e^{-1} = 11$ with $\epsilon_e = 0.1$. In the non-relativistic case, we also apply a factor of $4^{1/17}$ and $4^{11/17}$ to R_{eq} and E_{eq} , respectively, as discussed by Barniol Duran et al. (2013).

Before discussing the physical constraints, we emphasize that our assumptions are not always accurate or appropriate. Differing conditions such as deviation from equipartition, $\eta > 1$, $z \neq 0.2$, and different jet structures (e.g., narrow jets with $f_A = f_V = (\theta_j \Gamma)^2$) will change

the exact values of the physical quantities. Examination of all possible variations in the parameters is beyond the scope of this study, and the numbers we show should be treated (at best) as order-of-magnitude estimates meant to lead the discussion.

In Figure 9, we show plots of $L_{\nu, \text{peak}}$ vs. ν_{peak} including lines of constant values of the derived physical quantities for various scenarios (labeled at the top left of each panel). The approximate region covered by our transient candidates is also shaded in orange for reference (but note that the shown borders are rough lower limits and the region can extend beyond the plot). In all scenarios, the dependence of the physical quantities is clear: a larger $L_{\nu, \text{peak}}$ indicates a larger E_{eq} , a larger R_{eq} , and a smaller n_{ext} , while a larger ν_{peak} indicates a smaller E_{eq} , a smaller R_{eq} , and a larger n_{ext} . Now, we examine the physical constraints associated with the inverted spectra of our transient candidates in each scenario and discuss potential implications.

Non-relativistic outflow: In panel (a) of Figure 9, we show the non-relativistic scenario. To produce the observed $L_{\nu, \text{peak}} \sim 10^{30} - 10^{33} \text{ erg s}^{-1} \text{ Hz}^{-1}$ at $\nu_{\text{peak}} \sim 1 - 10 \text{ GHz}$ (orange region), a non-relativistic ($\Gamma = 1$) outflow requires $E_{\text{eq}} \sim 10^{50} - 10^{53} \text{ erg}$ at $R_{\text{eq}} \sim 10^{17} - 10^{19} \text{ cm}$ with $n_{\text{ext}} \sim 1 \text{ cm}^{-3}$. This energy range is quite high, which is a direct result of the high luminosity over the low GHz frequency range. Unsurprisingly, it is consistent with (or even larger than) energies inferred from relativistic transients such as GRB afterglows and relativistic TDEs (Beniamini & van der Horst 2017; Eftekhari et al. 2018) and is (up to orders of magnitude) beyond those inferred from SNe, LFBOTs, and thermal TDEs (Coppejans et al. 2020; Ho et al. 2022; Christy et al. 2024). Such high energy simply reaffirms that we expect mainly the brightest and most energetic (extragalactic) transients to be selected in VLASS and VCSS based on inverted spectra because of the sensitivity limit (i.e., the sensitivity of VCSS requires a $\gtrsim 15 \text{ mJy}$ detection in VLASS).

The emission size is related to the timescale and the outflow velocity of the transient. For relativistic transients, we can crudely estimate the timescale assuming that the outflow velocity at the non-relativistic phase can be represented by an average velocity that is some fraction of the speed of light (which was the case for VT J0243-2840; Somalwar et al. 2023b). For the range $R_{\text{eq}} \sim 10^{17} - 10^{19} \text{ cm}$, we estimate a rough timescale of $t \approx R_{\text{eq}}(1+z)/\langle v \rangle \lesssim 1 - 100 \text{ yr}$ for $\langle v \rangle \gtrsim 0.1c$ (over the orange region). This range of emission size (and timescale) also overlaps with a density range of $n_{\text{ext}} \sim 10^{-2} - 10^0 \text{ cm}^{-3}$, and a smaller emission size generally corresponds to a larger density.

At the fainter end, our transient candidates with $L_{\nu, \text{peak}} \lesssim 10^{30} - 10^{31} \text{ erg s}^{-1} \text{ Hz}^{-1}$ peaking at more than a few GHz can be explained by relatively old non-relativistic outflows with reasonable energies of $E_{\text{eq}} \lesssim 10^{51} \text{ erg}$. These have been expanding for less than about

¹⁶ For the spectral index to be $\alpha > 0$ between two points at 340 MHz and 3.0 GHz, assuming the simplest case of two intersecting power laws (no curvature) with $\alpha = 2.5/ - 0.75$ below/above the peak (standard for synchrotron spectrum), we expect $\nu_{\text{peak}} > 562 \text{ MHz}$. Therefore, within an order of magnitude, our inverted spectra suggest $\nu_{\text{peak}} \gtrsim \text{GHz}$.

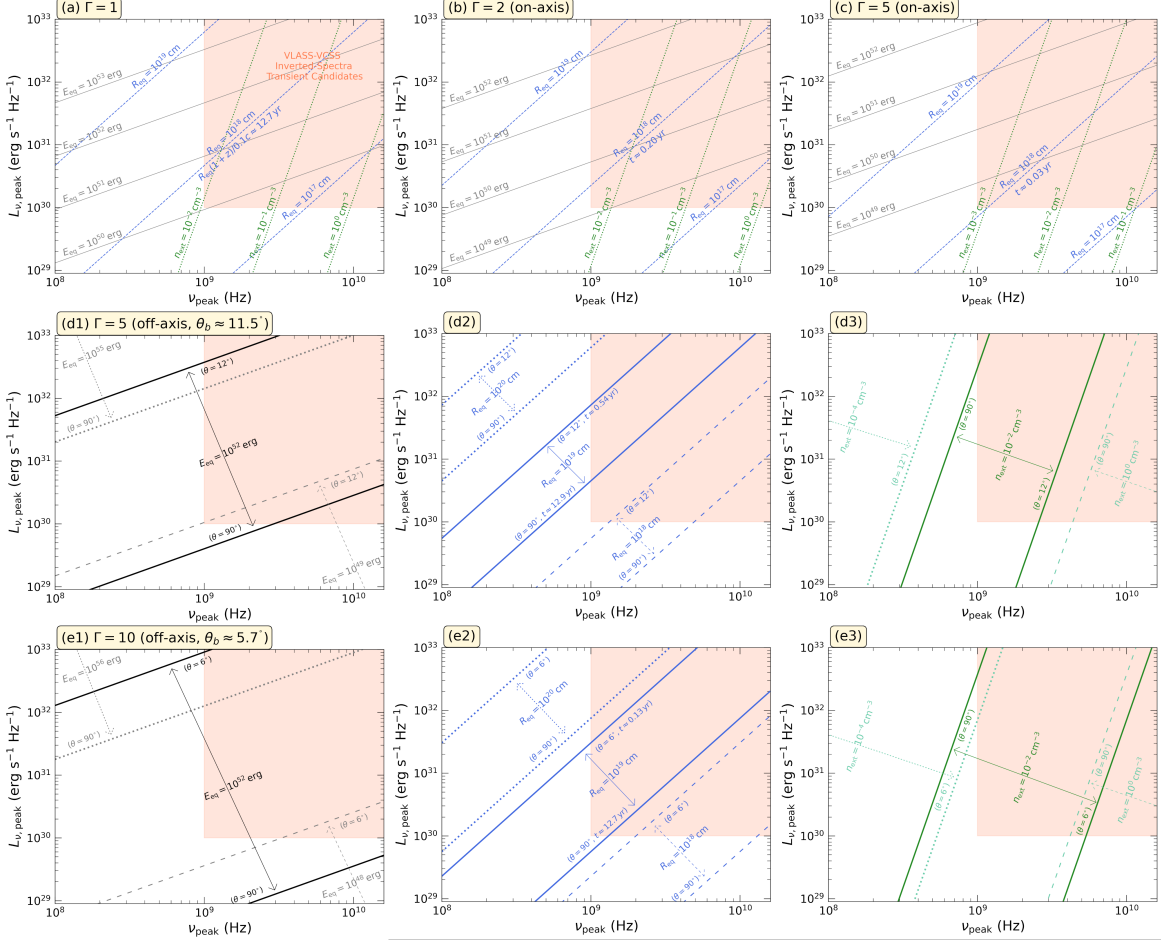


Figure 9. Plots of $L_{\nu, \text{peak}}$ vs. ν_{peak} showing physical quantities derived following Barniol Duran et al. (2013) and Matsumoto & Piran (2023) for various scenarios. The quantities, E_{eq} , R_{eq} , and n_{ext} , are shown as lines of constant values in gray, blue, and green, respectively. The derived time t for one value of R_{eq} is also shown for reference in each scenario (which scales linearly to other values of R_{eq}). The approximate region of phase space covered by our transient candidates is shaded in orange (but note that it can extend towards the top right). The label for each panel is placed at the top left with a description of the scenario. Panel (a) describes a non-relativistic outflow with $\Gamma = 1$. Panel (b) and (c) describe on-axis relativistic outflows with $\Gamma = 2$ and $\Gamma = 5$, respectively. Panels (d1), (d2), and (d3) describe the same off-axis outflow with $\Gamma = 5$ (and $\theta_b = \cos^{-1} \beta$ is the boundary dividing on-axis and off-axis cases) but show the three physical quantities separately for clarity. For the off-axis case, a constant quantity spans a range that corresponds to the range of θ . In our plots, we show three ranges spanned by arrows (labeled by the value of the quantity) and bounded by two lines with limiting values of θ (labeled at the left/right of the arrow for the lower/upper boundary). Only one boundary is shown with a lighter color when the other boundary is beyond the limits of our plots. Panels (e1), (e2), and (e3) are the same as panels (d1), (d2), and (d3), but with $\Gamma = 10$.

a decade and are now in low density environments with $n_{\text{ext}} \lesssim 1 \text{ cm}^{-3}$, which is also reasonable considering the large presumed distance from the galaxy centers (for comparison with circumnuclear densities inferred from TDEs, see Figure 9 in Christy et al. 2024). This result suggests that at this luminosity, it is possible to use an inverted spectrum in VLASS and VCSS to restrict the timescale of a transient at the non-relativistic phase to less than a decade old. If the spectral peak can be constrained to higher than a few GHz, perhaps through in-band spectral indices (e.g., a large positive α within the VLASS band), it may be possible to select less ener-

getic but even younger radio transients at an early stage of the non-relativistic phase. Therefore, in theory, an inverted spectrum from just one epoch of observation can be used to identify and motivate follow-up observations of radio transients that are potentially still young.

We note that towards the brighter end ($L_{\nu, \text{peak}} \gtrsim 10^{33} \text{ erg s}^{-1} \text{ Hz}^{-1}$), the inferred physical quantities can become unreasonable at low frequencies. Aside from the extremely high energy ($E_{\text{eq}} \gtrsim 10^{53} \text{ erg}$, approaching or exceeding the energy budget of a normal TDE), the timescale in this regime can be longer than many decades, which would be inconsistent with the NVSS

non-detection two decades ago. This could potentially be a problem for our three candidates with the highest estimated spectral luminosities – VT J0013-3125, VT J1400+6413, VT J1757+2929 with $L_{3.0\text{GHz}} \gtrsim 10^{32} - 10^{33} \text{ erg s}^{-1} \text{ Hz}^{-1}$. However, they have $\nu_{\text{peak}} \gtrsim 3.0 \text{ GHz}$ (from the highly inverted SEDs seen in Figure 4), where the inferred energy and emission size can be much smaller and more reasonable. If there is inconsistency, it could be an indication that our model assumptions are not appropriate (e.g., the outflow may be relativistic with a smaller energy and timescale; see discussions of other panels of Figure 9 below) or an AGN origin is a more preferable explanation than a transient event at such high luminosity (perhaps supporting the case of highly inverted variable PS source discussed in Section 4.1.4). We are unable to make any conclusive arguments for either case considering model degeneracy and our limited observational constraints.

Lastly, we note that in theory, an inverted spectrum can provide strong constraints on the ambient density of radio transients. Unfortunately, the setup of VLASS and VCSS does not have sufficient depth or high enough frequency that would be useful for selecting radio transients in high density environments (such as the discovery by Dong et al. 2021). Nonetheless, the prospect of such utility of an inverted spectrum should be considered in future surveys that have much greater capabilities.

On-axis relativistic outflow: In panel (b) and (c) of Figure 9, we show the on-axis relativistic scenario. For this scenario, we consider two values of Lorentz factor, $\Gamma = 2$ and $\Gamma = 5$, motivated by the early Lorentz factor inferred from Swift J1644+57 (Eftekhari et al. 2018). We calculate the timescale using $t \approx R_{\text{eq}}(1 - \beta)(1 + z)/(\beta c)$, where $\beta = v/c$ (Barniol Duran et al. 2013). Compared to the non-relativistic case, lower E_{eq} is needed to produce the same brightness and the timescale is now much smaller at the same R_{eq} , especially with larger values of Γ . At the same peak luminosity and frequency, a larger Γ also leads to a larger R_{eq} and a smaller n_{ext} .

At high luminosities, the inferred E_{eq} and timescale is much more reasonable compared to the non-relativistic case. In general, it appears that our transient candidates can reasonably be explained by on-axis relativistic outflows. In this case, an inverted spectrum in theory provides an even stronger constraint on the age of the transient. However, we note that if the outflow was relativistic during VLASS epoch 1, it should have been decelerating over time in order to explain the observed inverted spectrum in epoch 2. If the outflow was not decelerating (constant Γ), at a constant E_{eq} , the expansion over $\gtrsim 3 \text{ yr}$ (leading to more than an order of magnitude increase in R_{eq} for $\Gamma = 2$) should result in a significant decrease in ν_{peak} , which was not observed in epoch 2. Alternatively, for a constant Γ , it may be possible to maintain an inverted spectrum if E_{eq} increases by multiple orders of magnitude (perhaps through energy

injection). However, the increase in energy would likely result in noticeable brightening, which was also not observed in epoch 2 for any of our transient candidates. Therefore, the natural explanation for the inverted spectrum observed in both VLASS epochs is deceleration of the outflow.

In the on-axis relativistic scenario, we note that the inferred ambient density can be quite low, especially for large values of Γ . For $\Gamma = 5$, at a high luminosity and low frequency (within the orange region), the density becomes $n_{\text{ext}} \lesssim 10^{-3} \text{ cm}^{-3}$, which perhaps is explainable by the hot ionized medium or dwarf galaxies devoid of gas (e.g., Putman et al. 2021). This density would be even lower for larger Γ , which could be an indication that such on-axis relativistic outflow cannot reasonably explain our transient candidates.

Off-axis relativistic outflow: In panels (d) and (e) of Figure 9, we show the off-axis scenario. We consider two values of Lorentz factor, $\Gamma = 5$ and $\Gamma = 10$, with the emission beamed away from the line of sight, i.e., viewing angles $\theta > \theta_b$ (up to 90°), where $\theta_b = \cos^{-1} \beta$ is the boundary between on-axis and off-axis angles (following Matsumoto & Piran 2023). We calculate the timescale using $t \approx R_{\text{eq}}(1 - \beta \cos \theta)(1 + z)/(\beta c)$, leading to larger t for larger θ . As expected, a higher energy is required to produce the same luminosity at a larger viewing angle. In general, at small viewing angles, the difference between the on-axis and off-axis case is small, and the inferred values of E_{eq} , R_{eq} , and n_{ext} are still reasonable, at least for small Γ .

At small values of Γ and relatively low luminosities, our transient candidates can also be reasonably explained by the edge-on ($\theta = 90^\circ$) case. For example, for $\Gamma = 5$ and $\theta = 90^\circ$, transients with $L_{\nu, \text{peak}} \sim 10^{30} - 10^{31} \text{ erg s}^{-1} \text{ Hz}^{-1}$ and $\nu_{\text{peak}} \sim 1 - 10 \text{ GHz}$ can be explained by an outflow with $E_{\text{eq}} \sim 10^{52} \text{ erg}$, $R_{\text{eq}} \sim 10^{18} \text{ cm}$ ($t \sim 1 \text{ yr}$), and $n_{\text{ext}} \sim 10^{-1} - 10^1 \text{ cm}^{-3}$. However, at higher luminosities of $L_{\nu, \text{peak}} \gtrsim 10^{32} \text{ erg s}^{-1} \text{ Hz}^{-1}$, the edge-on case requires an extremely high $E_{\text{eq}} \sim 10^{54} \text{ erg}$, which is potentially unphysical for an ordinary TDE. This problem is exacerbated at larger values of Γ , where larger E_{eq} is needed to produce the same luminosity. Thus, our transient candidates are less likely explained by off-axis outflows at large viewing angles moving at extreme velocities.

We note that the issue of low n_{ext} at high Γ also exists in the off-axis case, particularly for small viewing angles. For example, for $\Gamma = 10$ and a peak frequency in the low GHz range, the inferred ambient density is $n_{\text{ext}} \lesssim 10^{-4} - 10^{-3} \text{ cm}^{-3}$ at $\theta \approx \theta_b$. Thus, this again could be an indication that relativistic outflows with large Γ close to on-axis cannot reasonably explain our transient candidates.

In general, for the off-axis case, an inverted spectrum similarly constrains the possible E_{eq} , R_{eq} , and n_{ext} . However, with the introduction of θ and the resulting degeneracy, the constraints in this case is weaker (i.e.,

at a single point of $(\nu_{\text{peak}}, L_{\nu, \text{peak}})$, possible values of the physical parameters can span orders of magnitude over the range of θ). Unfortunately, breaking this degeneracy is not easy and would require additional inputs such as apparent velocity measured from very long baseline interferometry observations (Matsumoto & Piran 2023). If the viewing angle is unknown, the effectiveness of using inverted spectra for constraining physical parameters is limited.

4.3. Feasibility of Search Method

In this final discussion, we briefly reflect on the feasibility of our method for searching and selecting inverted-spectra transients, and consider caveats and possible improvements for future searches. Our method of transient search is based mainly on the non-detection in NVSS and detection in VLASS above a certain threshold. The two surveys span a temporal baseline of more than two decades, and since radio transients generally have much shorter timescales than this (Pietka et al. 2015), our search should in theory capture the instantaneous number of transients on the sky above the flux density threshold and associated with a (previously) radio-quiet host. After introducing additional criteria on compactness and spectral index and removing cataloged AGNs, we ended up with a sample of 22 inverted-spectra transient candidates. Conveniently, because of our high flux density threshold (15 mJy limited by the sensitivity of VCSS), VLASS detections are on average $\gtrsim 100\sigma$ and we are significantly less troubled by false positives due to random noise structures. However, the down side of the high threshold and additional search criteria is that our final sample of transient candidates is fairly small compared to the thousands of variable and transient sources that have been found in VLASS (D. Dong, private communication).

From RACS-mid measurements, we found that nine of our candidates have brightened by $\gtrsim 300\%$ – 4000% at 1.4 GHz after NVSS, confirming their transient nature (including extreme AGN brightening) and demonstrating the successful side of our transient search. However, seven of our candidates have RACS-mid measurements that are only $\sim 20\%$ – 80% brighter than the NVSS upper limits. For these candidates, (even if the chance may be slim) we cannot rule out extremely rare cases of highly inverted variable PS sources that were slightly fainter than the NVSS upper limit but happened to brighten moderately in VLASS and RACS-mid. Although these PS sources are interesting objects in themselves, they are not considered transient events. “Contamination” by such sources is possible because we have compared surveys at different frequencies, i.e., VLASS (3.0 GHz) and NVSS (1.4 GHz), and a difference in flux density can still be explained by an extraordinarily large spectral index. We note that it is difficult to estimate the expected number of PS sources in our sample due to the lack of robust statistics on variable PS sources with highly in-

verted spectra. Long-term monitoring will help distinguish real transient events from variable PS sources, as transients should evolve substantially over time.

Altogether, we conclude that our search is in general a success in identifying inverted-spectra transients, with the caveat that some fraction of the identified candidates may be contaminated by extremely rare PS sources. In future searches, the impact of such contamination can be reduced by raising the flux density threshold for VLASS such that connecting VLASS and NVSS would result in an unphysical spectral index. It is also possible to completely avoid such contamination by comparing between epochs of VLASS at the same frequency of 3.0 GHz (searches between epochs of VLASS is currently ongoing; D. Dong et al., in prep.).

Also, we originally designed our method to be robust rather than complete, resulting in a fairly small sample of transient candidates. However, in retrospect, it is possible to adjust the search criteria for a more complete search and a larger sample size. For example, the compactness criterion may be relaxed and slightly extended sources can also be examined for the possibility of being transient. In addition, rather than defining transient behavior based on non-detections in NVSS, a variability criterion would be better, because a previous non-detection is fundamentally the same as having a lower limit on the variability. In other words, we can define a transient to be any variable source above a certain variability threshold, which crudely mimics how transients are found through difference imaging (a better method but hard to carry out in our case). We leave these considerations for future searches, especially for later epochs of VLASS and VCSS.

5. SUMMARY & CONCLUSION

In this study, we presented our search for transients with inverted spectra ($\alpha > 0$) in epoch 1 of VLASS and VCSS. Our search resulted in 22 inverted-spectra transient candidates that are not associated with cataloged AGNs. To the best of our knowledge, none of our candidates have been reported as transients at other wavelengths. In searches of radio surveys, only one (VT 0243-2840) has been previously reported as a radio transient (Somalwar et al. 2023b). Many of our candidates have optical and IR counterparts, of which nine are matched to the centers of galaxies (Figure 3) that have photometric redshifts, while five candidates have no optical or IR counterparts. However, none of our candidates are matched to known stellar counterparts. We also searched for X-ray counterparts, which unfortunately yielded few results from available data and very limited constraints.

For our transient candidates, we compiled radio measurements from recent and ongoing radio surveys and constructed crude radio SEDs (Figure 4). All of our candidates with available measurements also show inverted spectra in epoch 2 of VLASS and VCSS. With RACS

measurements between VLASS and VCSS, assuming slow evolution over time, we found broadly two types of SEDs over $\nu \sim 0.8 - 3.0$ GHz: (i) highly inverted SEDs with $\alpha \sim 2.0 - 3.0$ that suggest $\nu_{\text{peak}} \gtrsim 3.0$ GHz and (ii) peaked SEDs that suggest $\nu_{\text{peak}} \lesssim 1.0 - 3.0$ GHz. The RACS measurements also confirmed in almost all cases that our candidates experienced some level ($\gtrsim 20\%$ – 4000%) of brightening after NVSS at 1.4 GHz. From the VLASS epoch 1 and 2 measurements, we found that most of our candidates experienced only marginal variability at 3.0 GHz between the two epochs, with the majority not being statistically significant (Figure 5). However, from searching ASKAP surveys, we found light curves for three of our candidates that showed smooth brightening over hundreds of days and no evidence for any sporadic variation (Figure 6).

Based on the results of our search, we considered possible classifications for our inverted-spectra transient candidates. From the high spectral luminosity of $L_{3.0\text{GHz}} \sim 10^{30} - 10^{33} \text{ erg s}^{-1} \text{ Hz}^{-1}$ and marginal variability over $t/(1 + z_{\text{phot}}) \gtrsim 500 - 900$ d, we disfavored non-relativistic transients (including SNe, LFBOs, and thermal TDEs) and GRB afterglows as plausible classifications for our candidates. We also disfavored in general Galactic transients due to the lack of any bright optical stellar counterparts, although we cannot completely rule out bright Galactic radio transients (e.g., classical novae) at large distances. We found the most plausible transient classification to be relativistic TDEs, especially considering the spatial coincidences with centers of galaxies. However, without optical spectral classifications and sufficient X-ray constraints, we were unable to fully rule out the presence of AGNs (presumably with weaker optical and IR emission) in any of the host galaxies. Thus, our transient candidates that brightened significantly (by $\gtrsim 300\%$ – 4000%) can still be explained by young jets launched by AGNs, while candidates that brightened at least marginally (by $\gtrsim 20\%$ – 80%) may be explainable by extremely rare cases of highly inverted variable PS sources.

Finally, we examined physical constraints associated with the inverted spectra from VLASS and VCSS following the equipartition analyses of Barniol Duran et al. (2013) and Matsumoto & Piran (2023). We found that our transient candidates can reasonably be explained by non-relativistic outflows, on-axis relativistic outflows, or off-axis relativistic outflows, but with some differences in the inferred energies, emission sizes, timescales, and ambient densities. In general, a high energy of $E_{\text{eq}} \gtrsim 10^{49} - 10^{53} \text{ erg}$ is required to produce the observed high luminosity. A peak frequency at $\nu_{\text{peak}} \gtrsim 1 - 10$ GHz would constrain the ambient density to $n_{\text{ext}} \gtrsim 10^{-3} - 10^0 \text{ cm}^{-3}$ and the outflow duration to months or years. We also noted that certain solutions could be unphysical for our transient candidates. For example, a high velocity (say $\Gamma > 10$) on-axis outflow could result in an unrealistically low ambient density

($n_{\text{ext}} \lesssim 10^{-4} - 10^{-3} \text{ cm}^{-3}$), and a high velocity outflow viewed edge on ($\theta = 90^\circ$) could result in a prohibitively large energy ($E_{\text{eq}} \gtrsim 10^{54} - 10^{56} \text{ erg}$). These solutions are perhaps an indication that our transient candidates are unlikely explainable by extremely fast outflows, particularly those viewed at large off-axis angles.

Overall, with the current setup of VLASS and VCSS, inverted spectra can be a useful criterion for selecting luminous relativistic radio transients, with potential applications for transient searches in epoch 2 and 3 of VLASS. This would also provide some constraints on timescale, ranging from months to years, although this is highly dependent on factors that are typically unknown during a transient search, such as the outflow velocity. Unfortunately, at high luminosities, the constraint on peak frequency ($\nu_{\text{peak}} \gtrsim 3$ GHz) is insufficient for distinguishing transients in high density environments. We also remarked that due to the degeneracy introduced by the viewing angle, the effectiveness of inverted spectra in constraining physical properties is limited. While there certainly is potential in the utility of spectral information in a transient search, its merit may perhaps be better realized in future surveys with much higher sensitivities conducted by next-generation facilities such as the SKA, the Deep Synoptic Array-2000, or possibly the next-generation VLA.

We thank Hannah Dykaar for catalog suggestions, and Biny Sebastian and Yjan Gordon for discussions about the VLASS catalog. Y.C. acknowledges support from the Natural Sciences and Engineering Research Council of Canada (NSERC) Canada Graduate Scholarships – Doctoral Program. K.R. thanks the LSST-DA Data Science Fellowship Program, which is funded by LSST-DA, the Brinson Foundation, and the Moore Foundation; Their participation in the program has benefited this work.

Basic research in radio astronomy at the U.S. Naval Research Laboratory (NRL) is supported by 6.1 Base funding. Construction and installation of VLITE was supported by the NRL Sustainment Restoration and Maintenance fund. The VLA is operated by the National Radio Astronomy Observatory (NRAO). The NRAO is a facility of the National Science Foundation operated under cooperative agreement by Associated Universities, Inc. CIRADA is funded by a grant from the Canada Foundation for Innovation 2017 Innovation Fund (Project 35999), as well as by the Provinces of Ontario, British Columbia, Alberta, Manitoba and Quebec. This research has made use of the Vizier catalogue access tool, CDS, Strasbourg, France (Ochsenbein 1996). The original description of the Vizier service was published in Ochsenbein et al. (2000).

This scientific work uses data obtained from Inyarrimanha Ilgari Bundara / the Murchison Radio-astronomy Observatory. We acknowledge the Wajarri Yamaji People as the Traditional Owners and native title holders of the Observatory site. CSIRO’s ASKAP radio telescope is part of the Australia Telescope National Facility (<https://ror.org/05qajvd42>). Operation of ASKAP is funded by the Australian Government with support from the National Collaborative Research Infrastructure Strategy. ASKAP uses the resources of the Pawsey Supercomputing Research Centre. Establishment of ASKAP, Inyarrimanha Ilgari Bundara, the CSIRO Murchison Radio-astronomy Observatory and the Pawsey Supercomputing Research Centre are initiatives of the Australian Government, with support from the Government of Western Australia and the Science and Industry Endowment Fund. This paper includes archived data obtained through the CSIRO ASKAP Science Data Archive, CASDA (<https://data.csiro.au>).

LOFAR data products were provided by the LOFAR Surveys Key Science project (LSKSP; <https://lofar-surveys.org/>) and were derived from observations with the International LOFAR Telescope (ILT). LOFAR is the Low Frequency Array designed and constructed by ASTRON. It has observing, data processing, and data storage facilities in several countries, which are owned by various parties (each with their own funding sources), and which are collectively operated by the ILT foundation under a joint scientific policy. The efforts of the LSKSP have benefited from funding from the European Research Council, NOVA, NWO, CNRS-INSU, the SURF Co-operative, the UK Science and Technology Funding Council and the Jülich Supercomputing Centre.

Facilities: VLA, ASKAP, LOFAR

Software: Astropy (Astropy Collaboration et al. 2013, 2018), TOPCAT (Taylor 2005), STILTS (Taylor 2006), NumPy (Harris et al. 2020), Matplotlib (Hunter 2007), SciPy (Virtanen et al. 2020).

APPENDIX

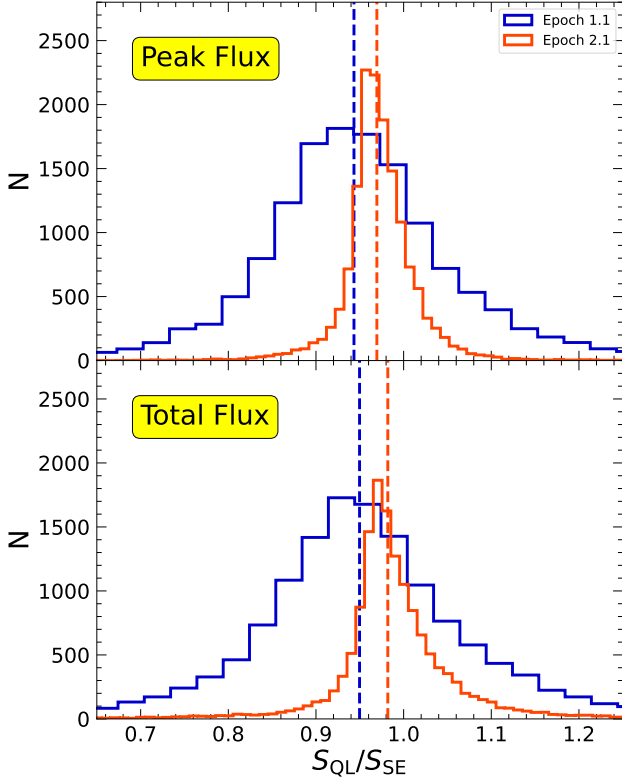


Figure 10. The distributions of the ratios of flux densities between the VLASS QL and SE sources, $S_{\text{QL}}/S_{\text{SE}}$. QL flux densities from epoch 1.1 (blue) and 2.1 (orange) are shown separately. The top and bottom panels show the ratios of peak flux density and total flux density, respectively. The medians of the distributions are shown with dashed lines. The underestimation of flux density in QL epoch 1.1 is worse compared to QL epoch 2.1 with significantly larger spread in distribution.

Table 6. Statistics of $S_{\text{QL}}/S_{\text{SE}}$

Epoch	Peak Flux		Total Flux	
	Median	MAD	Median	MAD
1.1	0.943	0.063	0.950	0.070
2.1	0.969	0.018	0.982	0.026

NOTE—MAD : median absolute deviation.

A. VLASS SYSTEMATIC FLUX DENSITY UNDERESTIMATION

Flux density measurements from the VLASS QL images are known to be systematically underestimated as a result of the imaging pipeline and residual phase and amplitude errors (Lacy et al. 2022b; Gordon et al. 2021). Additionally, this issue was worse for epoch 1.1 due to erroneous pointing offsets (Lacy et al. 2022b). Therefore, it is important to assess the systematic flux density underestimations in order to accurately compare the VLASS QL catalogs with other radio catalogs as well as between epochs.

To quantify the systematic underestimations, we directly compared the CIRADA VLASS QL catalogs used in this study (version 3 and 2 for epoch 1 and 2, respectively) with the CIRADA VLASS Single Epoch (SE) catalog (version 2) that covers $\sim 1000 \text{ deg}^2$ of the sky observed in epoch 2.1. The SE catalog was derived from higher quality VLASS images processed through the SE imaging pipeline with improved beam sampling, deeper cleaning, and self-calibration (Lacy et al. 2022a). The flux calibration accuracy of the SE images is known to be $\sim 3\%$, and therefore is suitable as a reference.

For the comparison, to minimize the impact of contamination, we followed the recommendations of the catalog User Guide (February 1, 2023 version) to select cleaner samples of the QL and SE catalogs. Specifically, the cleaner sample contains components with $Quality_flag = 0|4|8|12$, $P_sidelobe < 0.05$, $S_Code \neq E$, and $Duplicate_flag < 2$. Furthermore, we restricted the samples to sources relevant to this study, i.e., compact sources with $S_Code = S$ and $Maj < 5.0''$ as well as flux densities above the completeness limit of 3 mJy.

With the final samples, we cross-matched the QL and SE sources using a match radius of $2.0''$ and calculated the flux density ratio $S_{\text{QL}}/S_{\text{SE}}$. Since the SE catalog covers a part of epoch 2.1, the matched QL sources are almost exclusively from epoch 1.1 and 2.1, allowing us to characterize the underestimations in these two epochs. Figure 10 shows the the distributions of $S_{\text{QL}}/S_{\text{SE}}$ for both peak and total flux density. As expected, the underestimation of flux density in QL epoch 1.1 is worse than QL epoch 2.1 with a larger spread spread in distribution indicating significant uncertainty.

From these distributions, we derived the median and Median Absolute Deviation (MAD) values of $S_{\text{QL}}/S_{\text{SE}}$, given in Table 6. The median values imply that the flux density is underestimated by $\sim 5\%$ in QL epoch 1.1 and $\sim 2\% - 3\%$ in QL epoch 2.1. The MAD values indicate that the level of uncertainty is at $\sim 7\%$ in QL epoch 1.1 and $\lesssim 3\%$ in QL epoch 2.1. Note that although we could not make direct comparisons for QL epoch 1.2 and 2.2, the flux density accuracy at these epochs should be similar to QL epoch 2.1 (Lacy et al. 2022b). Therefore, for the VLASS QL catalogs used

in this study, we chose to correct the total flux density measurements by a factor of 1/0.95 for epoch 1.1 and by a factor of 1/0.98 for epoch 1.2+2.1+2.2. In addition,

we also added 7% and 3% of the total flux density measurements in quadrature to the uncertainties for epoch 1.1 and epoch 1.2+2.1+2.2, respectively.

REFERENCES

- Alexander, K. D., van Velzen, S., Horesh, A., & Zauderer, B. A. 2020, *SSRv*, 216, 81, doi: [10.1007/s11214-020-00702-w](https://doi.org/10.1007/s11214-020-00702-w)
- Allison, J. R., Sadler, E. M., Amaral, A. D., et al. 2022, *PASA*, 39, e010, doi: [10.1017/pasa.2022.3](https://doi.org/10.1017/pasa.2022.3)
- Almeida, A., Anderson, S. F., Argudo-Fernández, M., et al. 2023, *ApJS*, 267, 44, doi: [10.3847/1538-4365/acda98](https://doi.org/10.3847/1538-4365/acda98)
- An, T., & Baan, W. A. 2012, *ApJ*, 760, 77, doi: [10.1088/0004-637X/760/1/77](https://doi.org/10.1088/0004-637X/760/1/77)
- Anderson, M. M., Mooley, K. P., Hallinan, G., et al. 2020, *ApJ*, 903, 116, doi: [10.3847/1538-4357/abb94b](https://doi.org/10.3847/1538-4357/abb94b)
- Andreoni, I., Coughlin, M. W., Perley, D. A., et al. 2022, *Nature*, 612, 430, doi: [10.1038/s41586-022-05465-8](https://doi.org/10.1038/s41586-022-05465-8)
- Anumarlapudi, A., Dobie, D., Kaplan, D. L., et al. 2024, arXiv e-prints, arXiv:2407.12097, doi: [10.48550/arXiv.2407.12097](https://doi.org/10.48550/arXiv.2407.12097)
- Assef, R. J., Stern, D., Noirot, G., et al. 2018, *ApJS*, 234, 23, doi: [10.3847/1538-4365/aaa00a](https://doi.org/10.3847/1538-4365/aaa00a)
- Astropy Collaboration, Robitaille, T. P., Tollerud, E. J., et al. 2013, *A&A*, 558, A33, doi: [10.1051/0004-6361/201322068](https://doi.org/10.1051/0004-6361/201322068)
- Astropy Collaboration, Price-Whelan, A. M., Sipőcz, B. M., et al. 2018, *AJ*, 156, 123, doi: [10.3847/1538-3881/aabc4f](https://doi.org/10.3847/1538-3881/aabc4f)
- Atwood, W. B., Abdo, A. A., Ackermann, M., et al. 2009, *ApJ*, 697, 1071, doi: [10.1088/0004-637X/697/2/1071](https://doi.org/10.1088/0004-637X/697/2/1071)
- Bannister, K. W., Stevens, J., Tuntsov, A. V., et al. 2016, *Science*, 351, 354, doi: [10.1126/science.aac7673](https://doi.org/10.1126/science.aac7673)
- Barniol Duran, R., Nakar, E., & Piran, T. 2013, *ApJ*, 772, 78, doi: [10.1088/0004-637X/772/1/78](https://doi.org/10.1088/0004-637X/772/1/78)
- Barvainis, R., Lehár, J., Birkinshaw, M., Falcke, H., & Blundell, K. M. 2005, *ApJ*, 618, 108, doi: [10.1086/425859](https://doi.org/10.1086/425859)
- Beck, R., Szapudi, I., Flewelling, H., et al. 2021, *MNRAS*, 500, 1633, doi: [10.1093/mnras/staa2587](https://doi.org/10.1093/mnras/staa2587)
- Becker, R. H., White, R. L., & Helfand, D. J. 1995, *ApJ*, 450, 559, doi: [10.1086/176166](https://doi.org/10.1086/176166)
- Bellm, E. C., Kulkarni, S. R., Graham, M. J., et al. 2019, *PASP*, 131, 018002, doi: [10.1088/1538-3873/aaecbe](https://doi.org/10.1088/1538-3873/aaecbe)
- Beniamini, P., & van der Horst, A. J. 2017, *MNRAS*, 472, 3161, doi: [10.1093/mnras/stx2203](https://doi.org/10.1093/mnras/stx2203)
- Berger, E., Zauderer, A., Pooley, G. G., et al. 2012, *ApJ*, 748, 36, doi: [10.1088/0004-637X/748/1/36](https://doi.org/10.1088/0004-637X/748/1/36)
- Best, W. M. J., Magnier, E. A., Liu, M. C., et al. 2018, *ApJS*, 234, 1, doi: [10.3847/1538-4365/aa9982](https://doi.org/10.3847/1538-4365/aa9982)
- Bicknell, G. V., Mukherjee, D., Wagner, A. Y., Sutherland, R. S., & Nesvadba, N. P. H. 2018, *MNRAS*, 475, 3493, doi: [10.1093/mnras/sty070](https://doi.org/10.1093/mnras/sty070)
- Bietenholz, M. F., Bartel, N., Argo, M., et al. 2021, *ApJ*, 908, 75, doi: [10.3847/1538-4357/abccd9](https://doi.org/10.3847/1538-4357/abccd9)
- Bloom, J. S., Frail, D. A., & Kulkarni, S. R. 2003, *ApJ*, 594, 674, doi: [10.1086/377125](https://doi.org/10.1086/377125)
- Bloom, J. S., Giannios, D., Metzger, B. D., et al. 2011, *Science*, 333, 203, doi: [10.1126/science.1207150](https://doi.org/10.1126/science.1207150)
- Boella, G., Butler, R. C., Perola, G. C., et al. 1997, *A&AS*, 122, 299, doi: [10.1051/aas:1997136](https://doi.org/10.1051/aas:1997136)
- Bright, J. S., Margutti, R., Matthews, D., et al. 2022, *ApJ*, 926, 112, doi: [10.3847/1538-4357/ac4506](https://doi.org/10.3847/1538-4357/ac4506)
- Brown, G. C., Levan, A. J., Stanway, E. R., et al. 2015, *MNRAS*, 452, 4297, doi: [10.1093/mnras/stv1520](https://doi.org/10.1093/mnras/stv1520)
- . 2017, *MNRAS*, 472, 4469, doi: [10.1093/mnras/stx2193](https://doi.org/10.1093/mnras/stx2193)
- Burrows, D. N., Kennea, J. A., Ghisellini, G., et al. 2011, *Nature*, 476, 421, doi: [10.1038/nature10374](https://doi.org/10.1038/nature10374)
- Callingham, J. R., Gaensler, B. M., Ekers, R. D., et al. 2015, *ApJ*, 809, 168, doi: [10.1088/0004-637X/809/2/168](https://doi.org/10.1088/0004-637X/809/2/168)
- Callingham, J. R., Ekers, R. D., Gaensler, B. M., et al. 2017, *ApJ*, 836, 174, doi: [10.3847/1538-4357/836/2/174](https://doi.org/10.3847/1538-4357/836/2/174)
- Cameron, P. B., Chandra, P., Ray, A., et al. 2005, *Nature*, 434, 1112, doi: [10.1038/nature03605](https://doi.org/10.1038/nature03605)
- Cendes, Y., Eftekhari, T., Berger, E., & Polisensky, E. 2021, *ApJ*, 908, 125, doi: [10.3847/1538-4357/abd323](https://doi.org/10.3847/1538-4357/abd323)
- Cendes, Y., Berger, E., Alexander, K. D., et al. 2022, *ApJ*, 938, 28, doi: [10.3847/1538-4357/ac88d0](https://doi.org/10.3847/1538-4357/ac88d0)
- . 2023, arXiv e-prints, arXiv:2308.13595, doi: [10.48550/arXiv.2308.13595](https://doi.org/10.48550/arXiv.2308.13595)
- Cenko, S. B., Frail, D. A., Harrison, F. A., et al. 2011, *ApJ*, 732, 29, doi: [10.1088/0004-637X/732/1/29](https://doi.org/10.1088/0004-637X/732/1/29)
- Cenko, S. B., Krimm, H. A., Horesh, A., et al. 2012, *ApJ*, 753, 77, doi: [10.1088/0004-637X/753/1/77](https://doi.org/10.1088/0004-637X/753/1/77)
- Chambers, K. C., Magnier, E. A., Metcalfe, N., et al. 2016, arXiv e-prints, arXiv:1612.05560, doi: [10.48550/arXiv.1612.05560](https://doi.org/10.48550/arXiv.1612.05560)
- Chandra, P., & Frail, D. A. 2012, *ApJ*, 746, 156, doi: [10.1088/0004-637X/746/2/156](https://doi.org/10.1088/0004-637X/746/2/156)
- Chevalier, R. A. 1998, *ApJ*, 499, 810, doi: [10.1086/305676](https://doi.org/10.1086/305676)
- Chomiuk, L., Linford, J. D., Aydi, E., et al. 2021, *ApJS*, 257, 49, doi: [10.3847/1538-4365/ac24ab](https://doi.org/10.3847/1538-4365/ac24ab)
- Chrimes, A. A., Gompertz, B. P., Kann, D. A., et al. 2022, *MNRAS*, 515, 2591, doi: [10.1093/mnras/stac1796](https://doi.org/10.1093/mnras/stac1796)

- Christy, C. T., Alexander, K. D., Cendes, Y., et al. 2024, arXiv e-prints, arXiv:2404.12431, doi: [10.48550/arXiv.2404.12431](https://doi.org/10.48550/arXiv.2404.12431)
- Cifuentes, C., Caballero, J. A., Cortés-Contreras, M., et al. 2020, *A&A*, 642, A115, doi: [10.1051/0004-6361/202038295](https://doi.org/10.1051/0004-6361/202038295)
- Clarke, T. E., Kassim, N. E., Briskin, W., et al. 2016, in Society of Photo-Optical Instrumentation Engineers (SPIE) Conference Series, Vol. 9906, Ground-based and Airborne Telescopes VI, ed. H. J. Hall, R. Gilmozzi, & H. K. Marshall, 99065B, doi: [10.1117/12.2233036](https://doi.org/10.1117/12.2233036)
- Colless, M., Dalton, G., Maddox, S., et al. 2001, *MNRAS*, 328, 1039, doi: [10.1046/j.1365-8711.2001.04902.x](https://doi.org/10.1046/j.1365-8711.2001.04902.x)
- Condon, J. J., Cotton, W. D., Greisen, E. W., et al. 1998, *AJ*, 115, 1693, doi: [10.1086/300337](https://doi.org/10.1086/300337)
- Coppejans, D. L., Margutti, R., Terreran, G., et al. 2020, *ApJL*, 895, L23, doi: [10.3847/2041-8213/ab8cc7](https://doi.org/10.3847/2041-8213/ab8cc7)
- Cutri, R. M., Wright, E. L., Conrow, T., et al. 2021, *VizieR Online Data Catalog*, II/328
- Czerny, B., Siemiginowska, A., Janiuk, A., Nikiel-Wroczyński, B., & Stawarz, L. 2009, *ApJ*, 698, 840, doi: [10.1088/0004-637X/698/1/840](https://doi.org/10.1088/0004-637X/698/1/840)
- D’Abrusco, R., Massaro, F., Paggi, A., et al. 2013, *ApJS*, 206, 12, doi: [10.1088/0067-0049/206/2/12](https://doi.org/10.1088/0067-0049/206/2/12)
- Dálya, G., Díaz, R., Bouchet, F. R., et al. 2022, *MNRAS*, 514, 1403, doi: [10.1093/mnras/stac1443](https://doi.org/10.1093/mnras/stac1443)
- Davis, I., Hallinan, G., Ayala, C., Dong, D., & Myers, S. 2024, arXiv e-prints, arXiv:2408.14612, doi: [10.48550/arXiv.2408.14612](https://doi.org/10.48550/arXiv.2408.14612)
- de Gasperin, F., Williams, W. L., Best, P., et al. 2021, *A&A*, 648, A104, doi: [10.1051/0004-6361/202140316](https://doi.org/10.1051/0004-6361/202140316)
- de Gasperin, F., Edler, H. W., Williams, W. L., et al. 2023, *A&A*, 673, A165, doi: [10.1051/0004-6361/202245389](https://doi.org/10.1051/0004-6361/202245389)
- de Ruiter, I., Leseigneur, G., Rowlinson, A., et al. 2021, *MNRAS*, 508, 2412, doi: [10.1093/mnras/stab2695](https://doi.org/10.1093/mnras/stab2695)
- de Ruiter, I., Meyers, Z. S., Rowlinson, A., et al. 2023, arXiv e-prints, arXiv:2311.07394, doi: [10.48550/arXiv.2311.07394](https://doi.org/10.48550/arXiv.2311.07394)
- de Vries, W. H., Barthel, P. D., & O’Dea, C. P. 1997, *A&A*, 321, 105
- Dey, A., Schlegel, D. J., Lang, D., et al. 2019, *AJ*, 157, 168, doi: [10.3847/1538-3881/ab089d](https://doi.org/10.3847/1538-3881/ab089d)
- Dong, D. Z., & Hallinan, G. 2023, *ApJ*, 948, 119, doi: [10.3847/1538-4357/acc06c](https://doi.org/10.3847/1538-4357/acc06c)
- Dong, D. Z., Hallinan, G., Nakar, E., et al. 2021, *Science*, 373, 1125, doi: [10.1126/science.abg6037](https://doi.org/10.1126/science.abg6037)
- Duchesne, S. W., Grundy, J. A., Heald, G. H., et al. 2023a, arXiv e-prints, arXiv:2311.12369, <https://arxiv.org/abs/2311.12369>
- Duchesne, S. W., Thomson, A. J. M., Pritchard, J., et al. 2023b, *PASA*, 40, e034, doi: [10.1017/pasa.2023.31](https://doi.org/10.1017/pasa.2023.31)
- Duncan, K. J. 2022, *MNRAS*, 512, 3662, doi: [10.1093/mnras/stac608](https://doi.org/10.1093/mnras/stac608)
- Dykaar, H., Drout, M. R., Gaensler, B. M., et al. 2024, arXiv e-prints, arXiv:2406.08371, doi: [10.48550/arXiv.2406.08371](https://doi.org/10.48550/arXiv.2406.08371)
- Eftekhari, T., Berger, E., Zauderer, B. A., Margutti, R., & Alexander, K. D. 2018, *ApJ*, 854, 86, doi: [10.3847/1538-4357/aaa8e0](https://doi.org/10.3847/1538-4357/aaa8e0)
- Evans, I. N., Primini, F. A., Glotfelty, K. J., et al. 2010, *ApJS*, 189, 37, doi: [10.1088/0067-0049/189/1/37](https://doi.org/10.1088/0067-0049/189/1/37)
- Evans, P. A., Page, K. L., Beardmore, A. P., et al. 2023, *MNRAS*, 518, 174, doi: [10.1093/mnras/stac2937](https://doi.org/10.1093/mnras/stac2937)
- Evans, P. A., Page, K. L., Osborne, J. P., et al. 2020, *ApJS*, 247, 54, doi: [10.3847/1538-4365/ab7db9](https://doi.org/10.3847/1538-4365/ab7db9)
- Fassnacht, C. D., & Taylor, G. B. 2001, *AJ*, 122, 1661, doi: [10.1086/322112](https://doi.org/10.1086/322112)
- Flesch, E. W. 2019, arXiv e-prints, arXiv:1912.05614, doi: [10.48550/arXiv.1912.05614](https://doi.org/10.48550/arXiv.1912.05614)
- . 2021, arXiv e-prints, arXiv:2105.12985, doi: [10.48550/arXiv.2105.12985](https://doi.org/10.48550/arXiv.2105.12985)
- . 2023, arXiv e-prints, arXiv:2308.01505, doi: [10.48550/arXiv.2308.01505](https://doi.org/10.48550/arXiv.2308.01505)
- Fong, W., Berger, E., Margutti, R., & Zauderer, B. A. 2015, *ApJ*, 815, 102, doi: [10.1088/0004-637X/815/2/102](https://doi.org/10.1088/0004-637X/815/2/102)
- Fong, W.-f., Nugent, A. E., Dong, Y., et al. 2022, *ApJ*, 940, 56, doi: [10.3847/1538-4357/ac91d0](https://doi.org/10.3847/1538-4357/ac91d0)
- Gaensler, B. M., Kouveliotou, C., Gelfand, J. D., et al. 2005, *Nature*, 434, 1104, doi: [10.1038/nature03498](https://doi.org/10.1038/nature03498)
- Gaia Collaboration, Prusti, T., de Bruijne, J. H. J., et al. 2016, *A&A*, 595, A1, doi: [10.1051/0004-6361/201629272](https://doi.org/10.1051/0004-6361/201629272)
- Gaia Collaboration, Vallenari, A., Brown, A. G. A., et al. 2023, *A&A*, 674, A1, doi: [10.1051/0004-6361/202243940](https://doi.org/10.1051/0004-6361/202243940)
- Gao, H., Lei, W.-H., Zou, Y.-C., Wu, X.-F., & Zhang, B. 2013, *NewAR*, 57, 141, doi: [10.1016/j.newar.2013.10.001](https://doi.org/10.1016/j.newar.2013.10.001)
- Gehrels, N., Chincarini, G., Giommi, P., et al. 2004, *ApJ*, 611, 1005, doi: [10.1086/422091](https://doi.org/10.1086/422091)
- Goodwin, A. J., Alexander, K. D., Miller-Jones, J. C. A., et al. 2023, *MNRAS*, 522, 5084, doi: [10.1093/mnras/stad1258](https://doi.org/10.1093/mnras/stad1258)
- Gordon, Y. A., Boyce, M. M., O’Dea, C. P., et al. 2021, *ApJS*, 255, 30, doi: [10.3847/1538-4365/ac05c0](https://doi.org/10.3847/1538-4365/ac05c0)
- Górski, K. M., Hivon, E., Banday, A. J., et al. 2005, *ApJ*, 622, 759, doi: [10.1086/427976](https://doi.org/10.1086/427976)
- Granot, J., & Sari, R. 2002, *ApJ*, 568, 820, doi: [10.1086/338966](https://doi.org/10.1086/338966)
- Güdel, M. 2002, *ARA&A*, 40, 217, doi: [10.1146/annurev.astro.40.060401.093806](https://doi.org/10.1146/annurev.astro.40.060401.093806)

- Guillochon, J., Parrent, J., Kelley, L. Z., & Margutti, R. 2017, *ApJ*, 835, 64, doi: [10.3847/1538-4357/835/1/64](https://doi.org/10.3847/1538-4357/835/1/64)
- Gulati, A., Murphy, T., Kaplan, D. L., et al. 2023, *PASA*, 40, e025, doi: [10.1017/pasa.2023.21](https://doi.org/10.1017/pasa.2023.21)
- Hale, C. L., McConnell, D., Thomson, A. J. M., et al. 2021, *PASA*, 38, e058, doi: [10.1017/pasa.2021.47](https://doi.org/10.1017/pasa.2021.47)
- Hancock, P. J. 2009, *Astronomische Nachrichten*, 330, 180, doi: [10.1002/asna.200811151](https://doi.org/10.1002/asna.200811151)
- Harris, C. R., Millman, K. J., van der Walt, S. J., et al. 2020, *Nature*, 585, 357, doi: [10.1038/s41586-020-2649-2](https://doi.org/10.1038/s41586-020-2649-2)
- Hjellming, R. M., & Johnston, K. J. 1988, *ApJ*, 328, 600, doi: [10.1086/166318](https://doi.org/10.1086/166318)
- Ho, A. Y. Q., Phinney, E. S., Ravi, V., et al. 2019, *ApJ*, 871, 73, doi: [10.3847/1538-4357/aaf473](https://doi.org/10.3847/1538-4357/aaf473)
- Ho, A. Y. Q., Perley, D. A., Kulkarni, S. R., et al. 2020, *ApJ*, 895, 49, doi: [10.3847/1538-4357/ab8bcf](https://doi.org/10.3847/1538-4357/ab8bcf)
- Ho, A. Y. Q., Margalit, B., Bremer, M., et al. 2022, *ApJ*, 932, 116, doi: [10.3847/1538-4357/ac4e97](https://doi.org/10.3847/1538-4357/ac4e97)
- Horesh, A., Cenko, S. B., & Arcavi, I. 2021a, *Nature Astronomy*, 5, 491, doi: [10.1038/s41550-021-01300-8](https://doi.org/10.1038/s41550-021-01300-8)
- Horesh, A., Sfaradi, I., Fender, R., et al. 2021b, *ApJL*, 920, L5, doi: [10.3847/2041-8213/ac25fe](https://doi.org/10.3847/2041-8213/ac25fe)
- Hotan, A. W., Bunton, J. D., Chippendale, A. P., et al. 2021, *PASA*, 38, e009, doi: [10.1017/pasa.2021.1](https://doi.org/10.1017/pasa.2021.1)
- Hunter, J. D. 2007, *Computing in Science and Engineering*, 9, 90, doi: [10.1109/MCSE.2007.55](https://doi.org/10.1109/MCSE.2007.55)
- Intema, H. T., Jagannathan, P., Mooley, K. P., & Frail, D. A. 2017, *A&A*, 598, A78, doi: [10.1051/0004-6361/201628536](https://doi.org/10.1051/0004-6361/201628536)
- Jankowski, F., van Straten, W., Keane, E. F., et al. 2018, *MNRAS*, 473, 4436, doi: [10.1093/mnras/stx2476](https://doi.org/10.1093/mnras/stx2476)
- Jauncey, D. L., King, E. A., Bignall, H. E., et al. 2003, *PASA*, 20, 151, doi: [10.1071/AS03023](https://doi.org/10.1071/AS03023)
- Johnston, S., Bailes, M., Bartel, N., et al. 2007, *PASA*, 24, 174, doi: [10.1071/AS07033](https://doi.org/10.1071/AS07033)
- Keim, M. A., Callingham, J. R., & Röttgering, H. J. A. 2019, *A&A*, 628, A56, doi: [10.1051/0004-6361/201936107](https://doi.org/10.1051/0004-6361/201936107)
- Kellermann, K. I., & Pauliny-Toth, I. I. K. 1981, *ARA&A*, 19, 373, doi: [10.1146/annurev.aa.19.090181.002105](https://doi.org/10.1146/annurev.aa.19.090181.002105)
- Koribalski, B. S., Staveley-Smith, L., Westmeier, T., et al. 2020, *Ap&SS*, 365, 118, doi: [10.1007/s10509-020-03831-4](https://doi.org/10.1007/s10509-020-03831-4)
- Kosmaczewski, E., Stawarz, L., Siemiginowska, A., et al. 2020, *ApJ*, 897, 164, doi: [10.3847/1538-4357/ab9b1f](https://doi.org/10.3847/1538-4357/ab9b1f)
- Kunert-Bajraszewska, M., Gawroński, M. P., Labiano, A., & Siemiginowska, A. 2010, *MNRAS*, 408, 2261, doi: [10.1111/j.1365-2966.2010.17271.x](https://doi.org/10.1111/j.1365-2966.2010.17271.x)
- Kunert-Bajraszewska, M., Wołowska, A., Mooley, K., Kharb, P., & Hallinan, G. 2020, *ApJ*, 897, 128, doi: [10.3847/1538-4357/ab9598](https://doi.org/10.3847/1538-4357/ab9598)
- Lacy, M., Patil, P., & Nyland, K. 2022a, VCLASS Project Memo #17: Characterization of VCLASS Single Epoch Continuum Validation Products, https://library.nrao.edu/public/memos/vla/vlass/VLASS_017.pdf
- Lacy, M., Baum, S. A., Chandler, C. J., et al. 2020, *PASP*, 132, 035001, doi: [10.1088/1538-3873/ab63eb](https://doi.org/10.1088/1538-3873/ab63eb)
- Lacy, M., Meyers, S. T., Chandler, C., et al. 2022b, VCLASS Project Memo #13: Pilot and Epoch 1 Quick Look Data Release (v2), https://library.nrao.edu/public/memos/vla/vlass/VLASS_013.pdf
- Law, C. J., Gaensler, B. M., Metzger, B. D., Ofek, E. O., & Sironi, L. 2018, *ApJL*, 866, L22, doi: [10.3847/2041-8213/aae5f3](https://doi.org/10.3847/2041-8213/aae5f3)
- Lazio, T. J. W., Waltman, E. B., Ghigo, F. D., et al. 2001, *ApJS*, 136, 265, doi: [10.1086/322531](https://doi.org/10.1086/322531)
- Leung, J. K., Murphy, T., Lenc, E., et al. 2023, *MNRAS*, 523, 4029, doi: [10.1093/mnras/stad1670](https://doi.org/10.1093/mnras/stad1670)
- Leung, J. K., Murphy, T., Ghirlanda, G., et al. 2021, *MNRAS*, 503, 1847, doi: [10.1093/mnras/stab326](https://doi.org/10.1093/mnras/stab326)
- Lonsdale, C. J., Lacy, M., Kimball, A. E., et al. 2015, *ApJ*, 813, 45, doi: [10.1088/0004-637X/813/1/45](https://doi.org/10.1088/0004-637X/813/1/45)
- Lu, W., Matsumoto, T., & Matzner, C. D. 2023, arXiv e-prints, arXiv:2310.15336, doi: [10.48550/arXiv.2310.15336](https://doi.org/10.48550/arXiv.2310.15336)
- Lyke, B. W., Higley, A. N., McLane, J. N., et al. 2020, *ApJS*, 250, 8, doi: [10.3847/1538-4365/aba623](https://doi.org/10.3847/1538-4365/aba623)
- Lyman, J. D., Levan, A. J., Tanvir, N. R., et al. 2017, *MNRAS*, 467, 1795, doi: [10.1093/mnras/stx220](https://doi.org/10.1093/mnras/stx220)
- Marcote, B., Nimmo, K., Salafia, O. S., et al. 2019, *ApJL*, 876, L14, doi: [10.3847/2041-8213/ab1aad](https://doi.org/10.3847/2041-8213/ab1aad)
- Margutti, R., Metzger, B. D., Chornock, R., et al. 2019, *ApJ*, 872, 18, doi: [10.3847/1538-4357/aafa01](https://doi.org/10.3847/1538-4357/aafa01)
- Marocco, F., Eisenhardt, P. R. M., Fowler, J. W., et al. 2021, *ApJS*, 253, 8, doi: [10.3847/1538-4365/abd805](https://doi.org/10.3847/1538-4365/abd805)
- Masci, F. J., Laher, R. R., Rusholme, B., et al. 2019, *PASP*, 131, 018003, doi: [10.1088/1538-3873/aae8ac](https://doi.org/10.1088/1538-3873/aae8ac)
- Mateos, S., Alonso-Herrero, A., Carrera, F. J., et al. 2012, *MNRAS*, 426, 3271, doi: [10.1111/j.1365-2966.2012.21843.x](https://doi.org/10.1111/j.1365-2966.2012.21843.x)
- Matsumoto, T., & Piran, T. 2023, *MNRAS*, 522, 4565, doi: [10.1093/mnras/stad1269](https://doi.org/10.1093/mnras/stad1269)
- McConnell, D., Hale, C. L., Lenc, E., et al. 2020, *PASA*, 37, e048, doi: [10.1017/pasa.2020.41](https://doi.org/10.1017/pasa.2020.41)
- Merloni, A., Heinz, S., & di Matteo, T. 2003, *MNRAS*, 345, 1057, doi: [10.1046/j.1365-2966.2003.07017.x](https://doi.org/10.1046/j.1365-2966.2003.07017.x)
- Merloni, A., Lamer, G., Liu, T., et al. 2024, *A&A*, 682, A34, doi: [10.1051/0004-6361/202347165](https://doi.org/10.1051/0004-6361/202347165)
- Metzger, B. D., Williams, P. K. G., & Berger, E. 2015, *ApJ*, 806, 224, doi: [10.1088/0004-637X/806/2/224](https://doi.org/10.1088/0004-637X/806/2/224)

- Mhaskey, M., Gopal-Krishna, Dabhade, P., et al. 2019a, MNRAS, 485, 2447, doi: [10.1093/mnras/stz335](https://doi.org/10.1093/mnras/stz335)
- Mhaskey, M., Gopal-Krishna, Paul, S., et al. 2019b, MNRAS, 489, 3506, doi: [10.1093/mnras/stz2379](https://doi.org/10.1093/mnras/stz2379)
- Mohan, N., & Rafferty, D. 2015, PyBDSF: Python Blob Detection and Source Finder, Astrophysics Source Code Library, record ascl:1502.007
- Mooley, K. P., Hallinan, G., Bourke, S., et al. 2016, ApJ, 818, 105, doi: [10.3847/0004-637X/818/2/105](https://doi.org/10.3847/0004-637X/818/2/105)
- Mooley, K. P., Margalit, B., Law, C. J., et al. 2022, ApJ, 924, 16, doi: [10.3847/1538-4357/ac3330](https://doi.org/10.3847/1538-4357/ac3330)
- Mukherjee, D., Bicknell, G. V., Sutherland, R., & Wagner, A. 2016, MNRAS, 461, 967, doi: [10.1093/mnras/stw1368](https://doi.org/10.1093/mnras/stw1368)
- Murphy, T., Sadler, E. M., Ekers, R. D., et al. 2010, MNRAS, 402, 2403, doi: [10.1111/j.1365-2966.2009.15961.x](https://doi.org/10.1111/j.1365-2966.2009.15961.x)
- Murphy, T., Chatterjee, S., Kaplan, D. L., et al. 2013, PASA, 30, e006, doi: [10.1017/pasa.2012.006](https://doi.org/10.1017/pasa.2012.006)
- Murphy, T., Kaplan, D. L., Stewart, A. J., et al. 2021, PASA, 38, e054, doi: [10.1017/pasa.2021.44](https://doi.org/10.1017/pasa.2021.44)
- Nyland, K., Dong, D. Z., Patil, P., et al. 2020, ApJ, 905, 74, doi: [10.3847/1538-4357/abc341](https://doi.org/10.3847/1538-4357/abc341)
- Ochsenbein, F. 1996, The VizieR database of astronomical catalogues, CDS, Centre de Données astronomiques de Strasbourg, doi: [10.26093/CDS/VIZIER](https://doi.org/10.26093/CDS/VIZIER)
- Ochsenbein, F., Bauer, P., & Marcout, J. 2000, A&AS, 143, 23, doi: [10.1051/aas:2000169](https://doi.org/10.1051/aas:2000169)
- O'Dea, C. P. 1998, PASP, 110, 493, doi: [10.1086/316162](https://doi.org/10.1086/316162)
- O'Dea, C. P., & Saikia, D. J. 2021, A&A Rv, 29, 3, doi: [10.1007/s00159-021-00131-w](https://doi.org/10.1007/s00159-021-00131-w)
- Onken, C. A., Wolf, C., Bessell, M. S., et al. 2019, PASA, 36, e033, doi: [10.1017/pasa.2019.27](https://doi.org/10.1017/pasa.2019.27)
- Orienti, M., & Dallacasa, D. 2012, MNRAS, 424, 532, doi: [10.1111/j.1365-2966.2012.21226.x](https://doi.org/10.1111/j.1365-2966.2012.21226.x)
- . 2020, MNRAS, 499, 1340, doi: [10.1093/mnras/staa2856](https://doi.org/10.1093/mnras/staa2856)
- Orienti, M., Dallacasa, D., & Stanghellini, C. 2007, A&A, 475, 813, doi: [10.1051/0004-6361:20078105](https://doi.org/10.1051/0004-6361:20078105)
- . 2010, MNRAS, 408, 1075, doi: [10.1111/j.1365-2966.2010.17179.x](https://doi.org/10.1111/j.1365-2966.2010.17179.x)
- Paciesas, W. S., Meegan, C. A., Pendleton, G. N., et al. 1999, ApJS, 122, 465, doi: [10.1086/313224](https://doi.org/10.1086/313224)
- Padovani, P. 2016, A&A Rv, 24, 13, doi: [10.1007/s00159-016-0098-6](https://doi.org/10.1007/s00159-016-0098-6)
- Padovani, P., Alexander, D. M., Assef, R. J., et al. 2017, A&A Rv, 25, 2, doi: [10.1007/s00159-017-0102-9](https://doi.org/10.1007/s00159-017-0102-9)
- Pasham, D. R., Cenko, S. B., Levan, A. J., et al. 2015, ApJ, 805, 68, doi: [10.1088/0004-637X/805/1/68](https://doi.org/10.1088/0004-637X/805/1/68)
- Patil, P., Nyland, K., Whittle, M., et al. 2020, ApJ, 896, 18, doi: [10.3847/1538-4357/ab9011](https://doi.org/10.3847/1538-4357/ab9011)
- Perley, R. A., Chandler, C. J., Butler, B. J., & Wrobel, J. M. 2011, ApJL, 739, L1, doi: [10.1088/2041-8205/739/1/L1](https://doi.org/10.1088/2041-8205/739/1/L1)
- Perlman, E. S., Meyer, E. T., Wang, Q. D., et al. 2022, ApJ, 925, 143, doi: [10.3847/1538-4357/ac3bba](https://doi.org/10.3847/1538-4357/ac3bba)
- Peters, W., Clarke, T., Giacintucci, S., Nyland, K., & Polisensky, E. 2022, The VLITE Commensal Sky Survey (VCSS) Epoch 1 Bright Catalog Release, https://ws.cadc-ccda.hia-ihp.nrc-cnrc.gc.ca/files/vault/cirada/VCSS_Catalogue/VCSS_Bright_Catalog_Memo.pdf
- Peters, W., Polisensky, E., Brisken, W., et al. 2021, in American Astronomical Society Meeting Abstracts, Vol. 53, American Astronomical Society Meeting Abstracts, 211.06
- Pietka, M., Fender, R. P., & Keane, E. F. 2015, MNRAS, 446, 3687, doi: [10.1093/mnras/stu2335](https://doi.org/10.1093/mnras/stu2335)
- Planck Collaboration, Aghanim, N., Akrami, Y., et al. 2020, A&A, 641, A6, doi: [10.1051/0004-6361/201833910](https://doi.org/10.1051/0004-6361/201833910)
- Polisensky, E., Das, B., Peters, W., et al. 2023, ApJ, 958, 152, doi: [10.3847/1538-4357/ad0295](https://doi.org/10.3847/1538-4357/ad0295)
- Polisensky, E., Richards, E., Clarke, T., Peters, W., & Kassim, N. 2019, in Astronomical Society of the Pacific Conference Series, Vol. 523, Astronomical Data Analysis Software and Systems XXVII, ed. P. J. Teuben, M. W. Pound, B. A. Thomas, & E. M. Warner, 441
- Polisensky, E., Lane, W. M., Hyman, S. D., et al. 2016, ApJ, 832, 60, doi: [10.3847/0004-637X/832/1/60](https://doi.org/10.3847/0004-637X/832/1/60)
- Pritchard, J., Murphy, T., Heald, G., et al. 2024, MNRAS, 529, 1258, doi: [10.1093/mnras/stae127](https://doi.org/10.1093/mnras/stae127)
- Putman, M. E., Zheng, Y., Price-Whelan, A. M., et al. 2021, ApJ, 913, 53, doi: [10.3847/1538-4357/abe391](https://doi.org/10.3847/1538-4357/abe391)
- Randall, K. E., Hopkins, A. M., Norris, R. P., et al. 2012, MNRAS, 421, 1644, doi: [10.1111/j.1365-2966.2012.20422.x](https://doi.org/10.1111/j.1365-2966.2012.20422.x)
- Ravi, V., Dykaar, H., Codd, J., et al. 2022, ApJ, 925, 220, doi: [10.3847/1538-4357/ac2b33](https://doi.org/10.3847/1538-4357/ac2b33)
- Rengelink, R. B., Tang, Y., de Bruyn, A. G., et al. 1997, A&AS, 124, 259, doi: [10.1051/aas:1997358](https://doi.org/10.1051/aas:1997358)
- Rhodes, L., Bright, J. S., Fender, R., et al. 2023, MNRAS, 521, 389, doi: [10.1093/mnras/stad344](https://doi.org/10.1093/mnras/stad344)
- Riggi, S., Umana, G., Trigilio, C., et al. 2024, PASA, 41, e029, doi: [10.1017/pasa.2024.26](https://doi.org/10.1017/pasa.2024.26)
- Rose, K., Horesh, A., Murphy, T., et al. 2024, arXiv e-prints, arXiv:2410.01375, doi: [10.48550/arXiv.2410.01375](https://doi.org/10.48550/arXiv.2410.01375)
- Ross, K., Hurley-Walker, N., Seymour, N., et al. 2022, MNRAS, 512, 5358, doi: [10.1093/mnras/stac819](https://doi.org/10.1093/mnras/stac819)
- Ross, K., Callingham, J. R., Hurley-Walker, N., et al. 2021, MNRAS, 501, 6139, doi: [10.1093/mnras/staa3795](https://doi.org/10.1093/mnras/staa3795)

- Rybicki, G. B., & Lightman, A. P. 1979, Radiative processes in astrophysics
- Santana, R., Barniol Duran, R., & Kumar, P. 2014, *ApJ*, 785, 29, doi: [10.1088/0004-637X/785/1/29](https://doi.org/10.1088/0004-637X/785/1/29)
- Sari, R., Piran, T., & Narayan, R. 1998, *ApJL*, 497, L17, doi: [10.1086/311269](https://doi.org/10.1086/311269)
- Schlaflly, E. F., Meisner, A. M., & Green, G. M. 2019, *ApJS*, 240, 30, doi: [10.3847/1538-4365/aafbea](https://doi.org/10.3847/1538-4365/aafbea)
- Sfaradi, I., Horesh, A., Sollerman, J., et al. 2023, arXiv e-prints, arXiv:2312.00131, doi: [10.48550/arXiv.2312.00131](https://doi.org/10.48550/arXiv.2312.00131)
- Sfaradi, I., Beniamini, P., Horesh, A., et al. 2024, *MNRAS*, 527, 7672, doi: [10.1093/mnras/stad3717](https://doi.org/10.1093/mnras/stad3717)
- Shimwell, T. W., Röttgering, H. J. A., Best, P. N., et al. 2017, *A&A*, 598, A104, doi: [10.1051/0004-6361/201629313](https://doi.org/10.1051/0004-6361/201629313)
- Shimwell, T. W., Tasse, C., Hardcastle, M. J., et al. 2019, *A&A*, 622, A1, doi: [10.1051/0004-6361/201833559](https://doi.org/10.1051/0004-6361/201833559)
- Shimwell, T. W., Hardcastle, M. J., Tasse, C., et al. 2022, *A&A*, 659, A1, doi: [10.1051/0004-6361/202142484](https://doi.org/10.1051/0004-6361/202142484)
- Shingles, L., Smith, K. W., Young, D. R., et al. 2021, *Transient Name Server AstroNote*, 7, 1
- Shklovsky, J. 1965, *Nature*, 206, 176, doi: [10.1038/206176b0](https://doi.org/10.1038/206176b0)
- Sironi, L., & Giannios, D. 2013, *ApJ*, 778, 107, doi: [10.1088/0004-637X/778/2/107](https://doi.org/10.1088/0004-637X/778/2/107)
- Smith, K., Güdel, M., & Audard, M. 2005, *A&A*, 436, 241, doi: [10.1051/0004-6361:20042054](https://doi.org/10.1051/0004-6361:20042054)
- Smith, K. W., Smartt, S. J., Young, D. R., et al. 2020, *PASP*, 132, 085002, doi: [10.1088/1538-3873/ab936e](https://doi.org/10.1088/1538-3873/ab936e)
- Snellen, I. A. G., Schilizzi, R. T., de Bruyn, A. G., et al. 1998, *A&AS*, 131, 435, doi: [10.1051/aas:1998281](https://doi.org/10.1051/aas:1998281)
- Somalwar, J. J., Ravi, V., Dong, D., et al. 2022, *ApJ*, 929, 184, doi: [10.3847/1538-4357/ac5e29](https://doi.org/10.3847/1538-4357/ac5e29)
- Somalwar, J. J., Ravi, V., & Lu, W. 2023a, arXiv e-prints, arXiv:2310.03795, doi: [10.48550/arXiv.2310.03795](https://doi.org/10.48550/arXiv.2310.03795)
- Somalwar, J. J., Ravi, V., Dong, D. Z., et al. 2023b, *ApJ*, 945, 142, doi: [10.3847/1538-4357/acbafc](https://doi.org/10.3847/1538-4357/acbafc)
- . 2023c, arXiv e-prints, arXiv:2310.03791, doi: [10.48550/arXiv.2310.03791](https://doi.org/10.48550/arXiv.2310.03791)
- Somalwar, J. J., Ravi, V., Yao, Y., et al. 2023d, arXiv e-prints, arXiv:2310.03782, doi: [10.48550/arXiv.2310.03782](https://doi.org/10.48550/arXiv.2310.03782)
- Stanghellini, C., O’Dea, C. P., Dallacasa, D., et al. 1998, *A&AS*, 131, 303, doi: [10.1051/aas:1998270](https://doi.org/10.1051/aas:1998270)
- Stroh, M. C., Terreran, G., Coppejans, D. L., et al. 2021, *ApJL*, 923, L24, doi: [10.3847/2041-8213/ac375e](https://doi.org/10.3847/2041-8213/ac375e)
- Taylor, M. B. 2005, in *Astronomical Society of the Pacific Conference Series*, Vol. 347, *Astronomical Data Analysis Software and Systems XIV*, ed. P. Shopbell, M. Britton, & R. Ebert, 29
- Taylor, M. B. 2006, in *Astronomical Society of the Pacific Conference Series*, Vol. 351, *Astronomical Data Analysis Software and Systems XV*, ed. C. Gabriel, C. Arviset, D. Ponz, & S. Enrique, 666
- Teboul, O., & Metzger, B. D. 2023, *ApJL*, 957, L9, doi: [10.3847/2041-8213/ad0037](https://doi.org/10.3847/2041-8213/ad0037)
- Tetarenko, B. E., Bahramian, A., Arnason, R. M., et al. 2016, *ApJ*, 825, 10, doi: [10.3847/0004-637X/825/1/10](https://doi.org/10.3847/0004-637X/825/1/10)
- Tingay, S. J., & de Kool, M. 2003, *AJ*, 126, 723, doi: [10.1086/376600](https://doi.org/10.1086/376600)
- Tinti, S., Dallacasa, D., de Zotti, G., Celotti, A., & Stanghellini, C. 2005, *A&A*, 432, 31, doi: [10.1051/0004-6361:20041620](https://doi.org/10.1051/0004-6361:20041620)
- Tonry, J. L., Denneau, L., Heinze, A. N., et al. 2018, *PASP*, 130, 064505, doi: [10.1088/1538-3873/aabadf](https://doi.org/10.1088/1538-3873/aabadf)
- Tornainen, I., Tornikoski, M., Teräsanta, H., Aller, M. F., & Aller, H. D. 2005, *A&A*, 435, 839, doi: [10.1051/0004-6361:20041886](https://doi.org/10.1051/0004-6361:20041886)
- Tubín-Arenas, D., Krumpel, M., Lamer, G., et al. 2024, *A&A*, 682, A35, doi: [10.1051/0004-6361/202346773](https://doi.org/10.1051/0004-6361/202346773)
- Ueda, Y., Akiyama, M., Hasinger, G., Miyaji, T., & Watson, M. G. 2014, *ApJ*, 786, 104, doi: [10.1088/0004-637X/786/2/104](https://doi.org/10.1088/0004-637X/786/2/104)
- van Breugel, W., Miley, G., & Heckman, T. 1984, *AJ*, 89, 5, doi: [10.1086/113480](https://doi.org/10.1086/113480)
- van Haarlem, M. P., Wise, M. W., Gunst, A. W., et al. 2013, *A&A*, 556, A2, doi: [10.1051/0004-6361/201220873](https://doi.org/10.1051/0004-6361/201220873)
- Virtanen, P., Gommers, R., Oliphant, T. E., et al. 2020, *Nature Methods*, 17, 261, doi: [10.1038/s41592-019-0686-2](https://doi.org/10.1038/s41592-019-0686-2)
- von Kienlin, A., Meegan, C. A., Paciesas, W. S., et al. 2020, *ApJ*, 893, 46, doi: [10.3847/1538-4357/ab7a18](https://doi.org/10.3847/1538-4357/ab7a18)
- Wagner, A. Y., & Bicknell, G. V. 2011, *ApJ*, 728, 29, doi: [10.1088/0004-637X/728/1/29](https://doi.org/10.1088/0004-637X/728/1/29)
- Walker, M. A. 1998, *MNRAS*, 294, 307, doi: [10.1046/j.1365-8711.1998.01238.x](https://doi.org/10.1046/j.1365-8711.1998.01238.x)
- Wang, Y., Murphy, T., Lenc, E., et al. 2023, *MNRAS*, 523, 5661, doi: [10.1093/mnras/stad1727](https://doi.org/10.1093/mnras/stad1727)
- Wang, Z., Murphy, T., Kaplan, D. L., et al. 2022, *MNRAS*, 516, 5972, doi: [10.1093/mnras/stac2542](https://doi.org/10.1093/mnras/stac2542)
- Webb, N. A., Coriat, M., Traulsen, I., et al. 2020, *A&A*, 641, A136, doi: [10.1051/0004-6361/201937353](https://doi.org/10.1051/0004-6361/201937353)
- Wolowska, A., Kunert-Bajraszewska, M., Mooley, K., & Hallinan, G. 2017, *Frontiers in Astronomy and Space Sciences*, 4, 38, doi: [10.3389/fspas.2017.00038](https://doi.org/10.3389/fspas.2017.00038)
- Wolowska, A., Kunert-Bajraszewska, M., Mooley, K. P., et al. 2021, *ApJ*, 914, 22, doi: [10.3847/1538-4357/abe62d](https://doi.org/10.3847/1538-4357/abe62d)
- Wright, E. L., Eisenhardt, P. R. M., Mainzer, A. K., et al. 2010, *AJ*, 140, 1868, doi: [10.1088/0004-6256/140/6/1868](https://doi.org/10.1088/0004-6256/140/6/1868)
- Wu, F., An, T., Baan, W. A., et al. 2013, *A&A*, 550, A113, doi: [10.1051/0004-6361/201219700](https://doi.org/10.1051/0004-6361/201219700)

- Wygoda, N., Waxman, E., & Frail, D. A. 2011, *ApJL*, 738, L23, doi: [10.1088/2041-8205/738/2/L23](https://doi.org/10.1088/2041-8205/738/2/L23)
- Yao, Y., Ravi, V., Gezari, S., et al. 2023, *ApJL*, 955, L6, doi: [10.3847/2041-8213/acf216](https://doi.org/10.3847/2041-8213/acf216)
- Zauderer, B. A., Berger, E., Margutti, R., et al. 2013, *ApJ*, 767, 152, doi: [10.1088/0004-637X/767/2/152](https://doi.org/10.1088/0004-637X/767/2/152)
- Zauderer, B. A., Berger, E., Soderberg, A. M., et al. 2011, *Nature*, 476, 425, doi: [10.1038/nature10366](https://doi.org/10.1038/nature10366)
- Zhang, B., & Mészáros, P. 2001, *ApJL*, 552, L35, doi: [10.1086/320255](https://doi.org/10.1086/320255)
- . 2002, *ApJ*, 566, 712, doi: [10.1086/338247](https://doi.org/10.1086/338247)
- Zhang, F., Shu, X., Sun, L., et al. 2022, *ApJ*, 938, 43, doi: [10.3847/1538-4357/ac8a9a](https://doi.org/10.3847/1538-4357/ac8a9a)
- Zhang, F., Shu, X., Yang, L., et al. 2024, *ApJL*, 962, L18, doi: [10.3847/2041-8213/ad1d61](https://doi.org/10.3847/2041-8213/ad1d61)